Chronology of glaciations in the Sierra Nevada, California, from [10]Be surface exposure dating

Dylan H. Rood [a,b,*], Douglas W. Burbank [a], Robert C. Finkel [c,d]

[a] Department of Earth Science, University of California, Santa Barbara, CA 93106, USA
[b] Center for Accelerator Mass Spectrometry, Lawrence Livermore National Laboratory, Livermore, CA 94550, USA
[c] CEREGE, Aix en Provence, France
[d] Department of Earth and Planetary Science, University of California, Berkeley, CA 94720, USA

ARTICLE INFO

ABSTRACT

We use [10]Be surface exposure dating to construct a high-resolution chronology of glacial fluctuations in the Sierra Nevada, California. Most previous studies focused on individual glaciated valleys, whereas our study compares chronologies developed throughout the range to identify regional patterns in the timing of glacier response to major climate changes. Sites throughout the range indicate Last Glacial Maximum retreat at 18.8 ± 1.9 ka (2σ) that suggests rather consistent changes in atmospheric variables, e.g., temperature and precipitation, throughout the range. The penultimate glacial retreat occurred at ca 145 ka. Our data suggest that the Sierra Nevada landscape is dominated by glacial features deposited during marine isotope stage (MIS) 2 and MIS 6. Deposits of previously recognized glaciations between circa 25 and 140 ka, e.g., MIS 4, Tenaya, early Tahoe, cannot be unequivocally identified. The timing of Sierra Nevada glacial retreat correlates well with other regional paleoclimate proxies in the Sierra Nevada, but differs significantly from paleoclimate proxies in other regions. Our dating results indicate that the onset of LGM retreat occurred several thousand years earlier in the Sierra Nevada than some glacial records in the western US.

1. Introduction

An understanding of the relative timing of regional climate patterns is key to predicting future climate changes. The timing of past changes provides insights into causes and effects of climate over timescales beyond observational records. High-precision records are required to establish feedbacks among terrestrial, marine and atmospheric systems. Improved paleoclimate models require both well-dated and spatially extensive data (Kohfeld and Harrison, 2000) that provide reliable indicators of past terrestrial responses to climate changes.

Geomorphic records of mountain glaciation are one of the most ubiquitous terrestrial climate archives. Glaciers are regionally extensive and globally distributed from low to high latitudes, e.g., Thackray et al. (2008). Alpine glaciers are especially important for their sensitivity to regional climate perturbations (Oerlemans, 2005; Owen et al., 2009). Glacier mass balance is directly linked to integrated climate variables, including melt-season temperature and accumulation-season precipitation (i.e., snowfall) (Porter, 2001). Changes in climate cause glacial responses, e.g., changes in terminus position, which leave a geomorphic record of climate change in the landscape that can be reconstructed and numerically dated, e.g., Owen et al. (2008).

Individual glaciers do not necessarily respond to climate changes in the same way. Glacier mass balance, and likewise position of the glacier terminus, is controlled by temperature and precipitation, but complicated by local atmospheric effects including cloudiness, wind, long- and short-wave radiation balances, turbulent fluxes of sensible and latent heat, and humidity (Huybers and Roe, 2009). Each glacier is also subject to local variables including bed slope, hypsometry, accumulation area, debris cover, and local shading (Anderson et al., 2006). Several factors can result in variability in the response among individual glaciers within the same regional climate regime, including non-climatic factors, e.g., surging glaciers or debris cover. Regional glacial responses rise above local background variability; such responses provide a snapshot of regional climate and by inference associated atmospheric processes.

Existing chronologies for alpine glaciers show complex spatial and temporal patterns (Gillespie and Molnar, 1995; Thackray et al., 2008; Clark et al., 2009). During the global Last Glacial Maximum

* Corresponding author. Center for Accelerator Mass Spectrometry, Lawrence Livermore National Laboratory, Livermore, CA 94550, USA. Tel.: +1 925 422 7378; fax: +1 925 423 7884.
E-mail address: rood5@llnl.gov (D.H. Rood).

(LGM), glaciers in some mountain ranges reached their maximum extents during times of insolation minima, e.g., westernmost Himalaya (Owen et al., 2008), southern Alaska (Briner and Kaufman, 2008), Hawaii (Pigati et al., 2008), corresponding to the peak of marine isotope stage 2 (MIS 2) at ∼21 ± 2 ka (Mix et al., 2001). Conversely, other mountain glaciers advanced to maximum limits either before the ice sheet maximum, e.g., tropical Andes (Smith et al., 2005, 2008), arctic Alaska (Briner and Kaufman, 2008), or during times of global deglaciation, e.g., western U.S. (Licciardi and Pierce, 2008). Also, asynchronous local last glacial maxima are identified within a mountain range, e.g., Yellowstone Plateau (Licciardi and Pierce, 2008), tropical Andes (Smith et al., 2005, 2008). The differences in these glacial records are primarily credited to regional variations in atmospheric circulation patterns, sea-surface temperatures, and moisture sources (Munroe et al., 2006; Licciardi and Pierce, 2008).

This study shows that the timing of moraine stabilization and abandonment of the glacial terminus for Sierra Nevada alpine glaciers in California was similar throughout the mountain range. We construct chronologies throughout the range in order to identify regional patterns in past climate. Similar behavior of mountain glaciers in the Sierra Nevada may suggest spatially consistent changes in temperature and precipitation. Conversely, regional variability, such as diachronous responses or spatial patterns, would suggest changes in regional forcings, e.g., migrating moisture sources (Benson et al., 2003). We address the timing of glaciations across the Sierra Nevada by constructing the first regionally extensive chronology using high-precision [10]Be surface exposure dating of Sierran glacial deposits of the last and penultimate glaciations.

1.1. Regional setting

The Sierra Nevada is the longest continuous mountain range in the conterminous United States and was extensively glaciated throughout the Quaternary. Due to its N–S orientation, length (∼700 km), and elevation (>4000 m), it forms a major orographic barrier that separates Pacific maritime and continental climate regimes over a broad range of latitude and longitude (36–40°N, 118–121°W). The climate of the Sierra Nevada is dominated by winter storm tracks delivered by the Pacific jet stream, a pattern linked to sea-surface temperatures associated with the California Current (Yamamoto et al., 2007). A significant N–S and E–W gradient in snowfall is present (Howat and Tulaczyk, 2005). Mean annual precipitation at 37°N ranges from ∼100 cm/yr at the crest of the range to ∼15 cm/yr at the Owens Valley floor on the eastern side.

Climate models and paleoclimate proxy records indicate that during the LGM the jet stream was displaced south of its current average position in response to the cold, elevated surface of the Laurentide Ice Sheet (Thompson et al., 1993; Bartlein et al., 1998). These models suggest that Sierra Nevada glaciers are sensitive to both precipitation and temperature, but that their expansion required significant precipitation increases during the LGM (Hostetler and Clark, 1997). During the LGM, the glacier equilibrium line altitude (ELA) was lowered ∼700 m from modern with an elevation gradient that increased southward ∼2 m/km (Burbank, 1991). Recent numerical simulations of the LGM climate suggest that 5.6 °C of cooling, twice the precipitation (200 cm/yr), and an ELA ∼220 m higher on the east flank of the range compared to the west flank were required to reconstruct the spatial extent of glaciers in the central Sierra Nevada (Kessler et al., 2006).

1.2. Previous work

Previous work in the Sierra Nevada established an allostratigraphy for glacial deposits based, in part, on relative dating

techniques. Blackwelder (1931) created the classic nomenclature for the Sierra Nevada consisting of four glaciations: McGee, Sherwin, Tahoe, and Tioga (in order of decreasing age). Sharp and Birman (1963) added two additional glaciations to the Blackwelder chronology: the Mono Basin (between the Tahoe and Sherwin) and Tenaya (between the Tahoe and Tioga). Some controversy persists about the presence or absence of some of these glaciations, e.g., Burke and Birkeland (1979) for Tenaya and Mono Basin. The history of thought and nomenclature is addressed in detail by Warhaftig and Birman (1965), Gillespie et al. (1999), Clark et al. (2003), and Phillips et al. (2009). Much of the debate was driven, at least in part, by the lack of absolute dating of past advances.

In the past two decades, new geochronologic data and techniques have improved our understanding of the timing of Sierra Nevada glaciations. Radiometrically calibrated proxy records from Owens and Searles Lakes (Bischoff et al., 1997; Menking et al., 1997; Bischoff and Cummins, 2001) and Devils Hole (Winograd et al., 2006) provide high-resolution Late Pleistocene paleoenvironmental records. These proxies yield some constraints on the timing of glaciations and water-balance records. However, surface exposure dating of moraines using cosmogenic nuclides, e.g., [10]Be and [36]Cl (Gosse and Phillips, 2001), allowed for the first direct dating of Sierra Nevada glacial deposits (Phillips et al., 1990, 1996; James et al., 2002; Benn et al., 2006; Schaefer et al., 2006; Phillips et al., 2009) rather than bounding ages, e.g., Gillespie (1982), Bursik and Gillespie (1993), Clark and Gillespie (1997), or proxies.

Phillips et al. (1990) was the first to apply surface exposure dating to Sierra Nevada glacial deposits. Early studies using [36]Cl suggested multiple glacial advances correlating with Heinrich events 2, 3, and 5 in the northern Atlantic (Phillips et al., 1996). Recently, Phillips et al. (2009) refined the [36]Cl chronology at Bishop Creek (Fig. 1) using updated production parameterizations. This study concluded that deposits previously mapped as individual advances were, in fact, compound features deposited during MIS 2 and 6. Their data also suggested correlation between Sierra Nevada glaciations and northern Atlantic proxy records, for example, Tioga 4 advances were suggested to be synchronous with the peak of Heinrich event 1. The authors also address the inherent uncertainties associated with [36]Cl dating methods, which could affect these correlations.

Few previous studies have used [10]Be to address the timing of Sierra Nevada glaciations. James et al. (2002) first applied [10]Be dating methods to glacial deposits in Bear Valley in the northern Sierra Nevada (Fig. 1). This work broadly correlated fluctuations in glaciers on the western side of the range to those deduced from [36]Cl results on the eastern side. Benn et al. (2006) dated an LGM moraine using [10]Be while investigating the relationship among glaciation, sediment transport, and alluvial and lacustrine deposition in the Owens Valley (Whitney Portal site, Fig. 1). Schaefer et al. (2006) dated a LGM moraine in Bloody Canyon (Fig. 1), and compared the age to other mid-latitude sites in the northern and southern hemispheres. Those results suggested synchronous interhemispheric response of mid-latitude glaciers to termination of the LGM. These previous studies from individual glaciers permit an initial overview of the spatial and temporal patterns of glaciation in the Sierra Nevada. They have not, however, been reevaluated with updated age calculation parameters, e.g., production rate, half-life, and scaling scheme.

1.3. [10]Be surface exposure dating

Recent improvements in chemistry (Merchel et al., 2008; Schaefer et al., 2009), accelerator mass spectrometry (AMS) techniques (Schaefer et al., 2009; Rood et al., 2010), and AMS reference standards (Nishiizumi et al., 2007) have improved the precision and
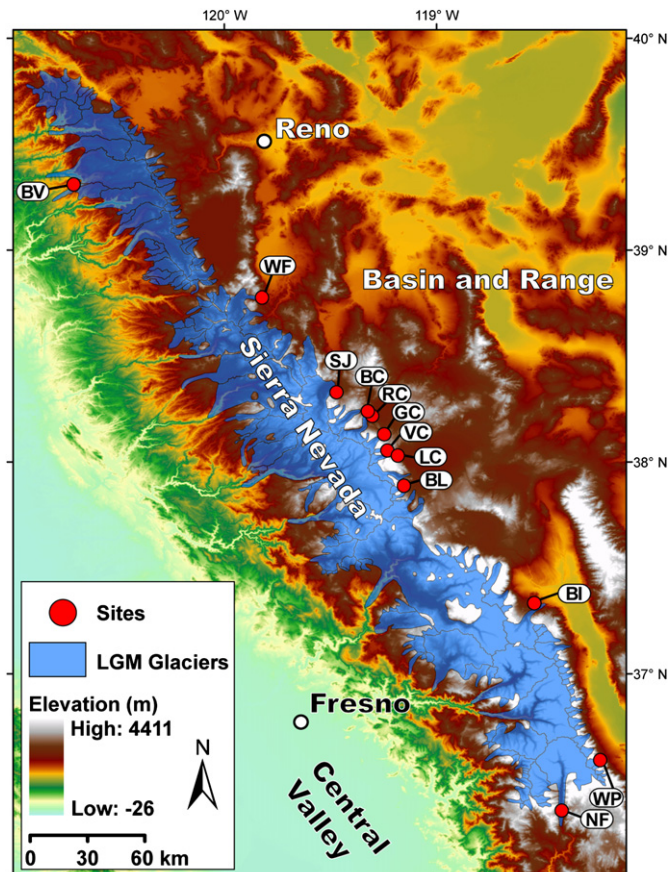
Fig. 1. Map of the Sierra Nevada showing elevation, LGM glacier extent, and study sites. Sites (from north to south): BV = Bear Valley, WF = Woodfords, SJ = Sonora Junction, BC = Buckeye Creek, RC = Robinson Creek, GC = Green Creek, LC = Lundy Canyon, BL = Bloody Canyon, BI = Bishop Creek, WP = Whitney Portal, and NF = Soda Springs.

accuracy of [10]Be analyses. Our ability to interpret accurate exposure ages has benefited from refinements of [10]Be production rates (Balco et al., 2009), half-life (Chmeleff et al., 2010; Korschinek et al., 2010), standardized age calculators (Balco et al., 2008), and spatial scaling schemes for cosmic ray flux and temporal variations due to changes in the geomagnetic field, e.g., Dunai (2001), Lifton et al. (2005), Desilets et al. (2006). Although disagreement still exists over [10]Be production rates, and the accuracy of ages are limited by both inheritance and erosion, these improvements have established [10]Be as the first tool available that allows us to compare detailed glacial chronologies with high confidence, e.g., Schaefer et al. (2009).

2. Methods

2.1. Mapping

Following the previous work of Clark (1967), Sharp (1972), Bursik (1989), and Ramelli et al. (1999), we mapped glacial moraines and outwash terraces in the Sonora Pass–Sonora Junction area (Fig. 2), the Bridgeport Basin, the Mono Basin, and in the Woodfords area (Fig. 1). Mapping was based on interpretation of stereoscopic pairs of black-and-white aerial photographs, high-resolution color orthoimagery (U.S. Department of Agriculture National Agriculture Imagery Program), and field observations. High-resolution color maps for each additional site and the individual boulder ages on each moraine are included in the supplemental materials (Figs. S1, S5, S7, S9, and S14). For simplicity, the

moraine nomenclature used by the original authors was retained. The glacial moraines and outwash terraces on which we focused our chronologic efforts were selected for their level of preservation, clear allostratigraphic relationships, and displacement across range-front faults for an accompanying neotectonic study (Rood et al., 2011). For surface exposure dating of LGM deposits, we sampled the outermost moraine from each sequence, which we interpret to indicate the timing of initial deglaciation.

2.2. Surface exposure dating

2.2.1. [10]Be ages

Information regarding field sampling methods, chemical processing, and AMS analyses is included in the supplemental data. The high precision of the measurements are the result of low background carrier and process blanks, low boron corrections, and high ion source beam currents. Exposure-age calculations were made with the CRONUS-Earth online exposure age calculator, Version 2.2 (hess.ess.washington.edu/math/) (Balco et al., 2008). Corrections for topographic shielding, surface geometry, and sample thickness corrections are <4%. Corrections for snow cover should be minimal (possibly 1–2%; Phillips et al., 2009) and are not applied. Individual surface boulder ages were not corrected for inheritance (discussed in Section 4.1.1).

Model exposure ages are calculated both with and without a correction for erosion. Given no *a priori* knowledge of each boulder's erosion rate, a range of rates is used. For zero erosion, model ages can be interpreted as *minimum* exposure ages. Erosion-corrected ages are calculated using maximum and preferred erosion rates of 3.1 m/Myr (Small et al., 1997) and 0.6 m/Myr, respectively. The ages presented in the data discussion and figures are calculated using our preferred erosion rate of 0.6 m/Myr (discussed further in Section 4.1.1).

Sample information, [10]Be concentrations, and model exposure ages are summarized in Table 1. [10]Be concentrations and model exposure ages of individual boulder samples are reported with 1σ analytical (internal) uncertainties (for the depth profile, the extrapolated surface [10]Be concentration was assigned a 5% uncertainty), which do not incorporate errors in sample thickness corrections, topographic shielding, and scaling. Age calculations using five different scaling schemes (Stone, 2000, after Lal, 1991; Dunai, 2001; Lifton et al., 2005; Desilets et al., 2006) are presented in the supplemental data (Table S1). Ages presented in the data discussion and figures are calculated using a constant production-rate model and a scaling scheme for spallation from Stone (2000) that is modified after Lal (1991). [10]Be data from James et al. (2002), Benn et al. (2006), Schaefer et al. (2006), and Amos et al. (2010) are recalculated using the same set of preferred inputs, e.g., erosion rate of 0.6 m/Myr.

2.2.2. [36]Cl ages

In order to directly compare the [36]Cl and [10]Be chronologies in the Sierra Nevada, we recalculate ages for the Bishop Creek dataset of Phillips et al. (2009) using the same input parameters as [10]Be age calculations, e.g., erosion rate, scaling scheme. [36]Cl ages are calculated using the online CRONUS [36]Cl Exposure Age Calculator (www.cronuscalculators.nmt.edu/cl-36/) using the Phillips et al. (2001) [36]Cl production rate parameterization.

2.2.3. Interpretation of landform exposure ages

For each moraine or outwash terrace, results for all samples are plotted together as a probability density function (PDF) diagram. Each sample is assigned a PDF defined by a Gaussian distribution with a mean and standard deviation from the age and 1σ analytical error. This approach allows testing whether analytical uncertainty,
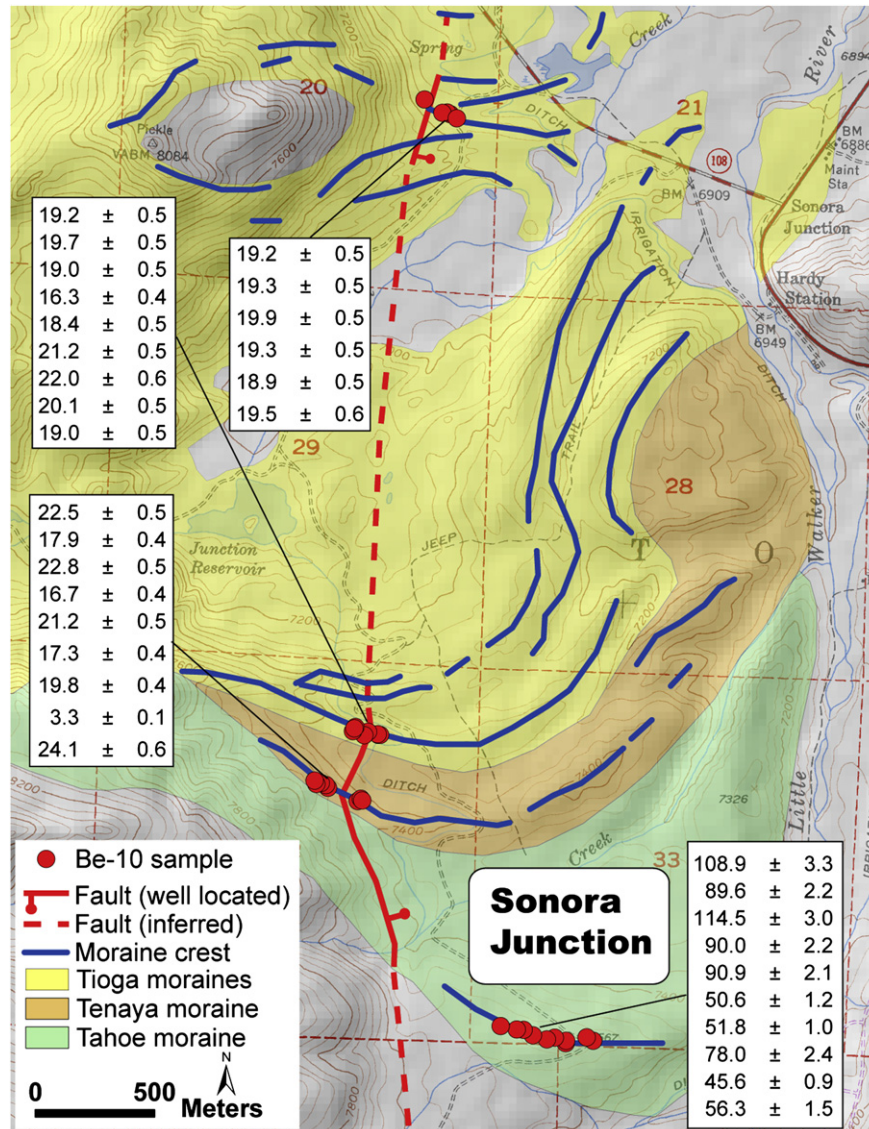
Fig. 2. Geomorphic map of the Sonora Junction (SJ) site (modified after Clark, 1967) showing glacial deposits, sample locations, and [10]Be ages.

derived from the normally distributed AMS counting statistics (Guilderson et al., 2003), is sufficient to explain the spread in the data. A cumulative probability density function is calculated by summing individual PDFs for all boulders from each deposit. Visual inspection of the cumulative PDF permits ready identification of groups and outliers in age distributions; peaks with a larger area under the curve are more likely to be the moraine stabilization age. Obvious outliers are identified in the cumulative PDF and excluded. A few old outlying ages are attributed to pre-depositional inheritance, whereas more frequent young outliers are interpreted to result from post-depositional exhumation, boulder erosion, or rotation.

Some deposits show a peak in the cumulative PDF that indicates a tight grouping of ages. In order to quantify the significance of the age peak, a reduced χ^2 (χ^2_R) statistic is calculated for the group within each PDF (Balco et al., 2009; Schaefer et al., 2009). The χ^2_R tests whether assigned age errors (i.e., analytical uncertainties) explain the observed scatter in the group. From the χ^2_R statistic, we calculate the probability (P) that the assigned age errors yield the observed amount of scatter or more. We chose a cutoff of $P > 0.05$ to indicate that the age errors alone explain the scatter in the dataset.

3. Results

A compilation of new and published [10]Be and [36]Cl surface exposure ages ($n = 229$) for the Sierra Nevada (Table 1) reveals moraine age estimates that we group as high, moderate, or low confidence based on the summary statistics (χ^2_R value and P) for each moraine or outwash surface (Table 2). Below we present examples for each confidence level from the Sonora Junction site (Figs. 2 and 3). Maps, field descriptions, PDF diagrams, and age interpretations for deposits in the remaining sites are included in the supplemental materials (Figs. S1–S29).

3.1. Examples from the Sonora junction site

The largest Pleistocene glaciers of the eastern slope of the Sierra Nevada occupied the West Walker River drainage near Sonora Pass (Sonora Junction site, Fig. 1). Previous work in the region indicates that at least four suites of glacial deposits are present (Clark, 1967; Clark et al., 2003), including Tioga, Tenaya, Tahoe, and Sherwin. Granitoid boulders of Fremont Lake granodiorite, Cathedral Peak granite, and Sonora Bridge quartz monzonite lithologies (Clark,

Table 1
^{10}Be concentrations and exposure ages.

Sample name	Latitude (DD)	Longitude (DD)	Elevation (m)	Thickness (cm) or *depth (cm)*	Shielding correction[a]	[^{10}Be] (10^3 atoms g^{-1})[b]	Standard	Minimum exposure age (ky)[c] erosion rate: 0	Maximum exposure age (ky)[d] erosion rate: 3.1 m/Myr	Preferred exposure age (ky)[e] erosion rate: 0.6 m/Myr
Robinson Creek Tahoe moraine										
RCTA05-1	38.2166	-119.3013	2100	2	0.999	3094.3 ± 47.6	KNSTD	141.2 ± 2.3	258.5 ± 9.1	152.5 ± 2.6
RCTA05-2	38.2157	-119.3016	2109	2	0.999	1173.2 ± 33.3	KNSTD	51.9 ± 1.5	60.5 ± 2.1	53.3 ± 1.6
RCTA05-3	38.2142	-119.3034	2094	1	0.997	2552.7 ± 61.1	KNSTD	115.6 ± 2.9	177.7 ± 7.4	123.0 ± 3.2
RCTA05-4	38.2145	-119.3029	2104	3	0.999	2499.6 ± 59.6	KNSTD	113.9 ± 2.8	173.5 ± 7.1	121.1 ± 3.2
RCTA05-5	38.2151	-119.3022	2111	1	0.997	2423.8 ± 63.3	KNSTD	108.3 ± 2.9	159.8 ± 6.8	114.7 ± 3.3
RCTA05-6	38.2164	-119.3013	2112	2	1.000	1192.2 ± 28.7	KNSTD	52.8 ± 1.3	61.7 ± 1.8	54.2 ± 1.4
RCTA05-7	38.2158	-119.3016	2107	1.5	0.999	2414.3 ± 75.4	KNSTD	108.3 ± 3.5	160.0 ± 8.2	114.8 ± 3.9
RCTA05-8	38.2158	-119.3016	2108	3	0.999	2743.2 ± 65.5	KNSTD	125.0 ± 3.1	203.6 ± 9.2	133.8 ± 3.5
RCTA05-9	38.2156	-119.3019	2106	1.5	0.999	1548.0 ± 51.2	KNSTD	68.8 ± 2.3	85.2 ± 3.6	71.3 ± 2.5
Sonora Junction Tioga moraine (southern lobe)										
SJTI05-1	38.3281	-119.4699	2246	2	0.998	475.0 ± 12.0	KNSTD	19.0 ± 0.5	20.0 ± 0.5	19.2 ± 0.5
SJTI05-2	38.3281	-119.4698	2247	2	0.999	486.3 ± 12.2	KNSTD	19.5 ± 0.5	20.5 ± 0.5	19.7 ± 0.5
SJTI05-3	38.3281	-119.4699	2248	2	0.999	470.8 ± 11.9	KNSTD	18.8 ± 0.5	19.8 ± 0.5	19.0 ± 0.5
SJTI05-4	38.3282	-119.4704	2252	3	0.999	403.0 ± 10.2	KNSTD	16.2 ± 0.4	16.9 ± 0.5	16.3 ± 0.4
SJTI05-5	38.3280	-119.4706	2251	3	0.996	451.2 ± 11.5	KNSTD	18.2 ± 0.5	19.1 ± 0.5	18.4 ± 0.5
SJTI05-6	38.3280	-119.4706	2251	1.5	0.999	528.3 ± 13.2	KNSTD	21.0 ± 0.5	22.2 ± 0.6	21.2 ± 0.5
SJTI05-7	38.3283	-119.4710	2257	3	0.998	540.9 ± 13.6	KNSTD	21.7 ± 0.6	23.1 ± 0.6	22.0 ± 0.6
SJTI05-8	38.3282	-119.4711	2256	3	0.998	494.2 ± 12.4	KNSTD	19.9 ± 0.5	20.9 ± 0.6	20.1 ± 0.5
SJTI05-9	38.3283	-119.4711	2253	1.5	0.998	472.3 ± 11.9	KNSTD	18.8 ± 0.5	19.7 ± 0.5	19.0 ± 0.5
Buckeye Creek Tahoe outwash terrace										
BCTA06-1	38.2379	-119.3213	2069	2	0.998	3288.1 ± 76.5	KNSTD	153.9 ± 3.7	316.3 ± 20.9	167.4 ± 4.4
BCTA06-2	38.2378	-119.3185	2121	5	0.996	3018.5 ± 57.6	KNSTD	139.5 ± 2.8	251.8 ± 10.8	150.5 ± 3.2
BCTA06-3	38.2379	-119.3181	2125	3	0.996	3053.8 ± 71.0	KNSTD	138.4 ± 3.3	247.8 ± 12.7	149.2 ± 3.9
BCTA06-4	38.2383	-119.3225	2123	3	0.999	2480.0 ± 51.9	KNSTD	111.5 ± 2.4	167.6 ± 5.9	118.4 ± 2.7
BCTA06-5	38.2382	-119.3224	2134	3	0.996	2253.6 ± 47.5	KNSTD	100.6 ± 2.2	142.9 ± 4.7	106.1 ± 2.4
BCTA06-6	38.2377	-119.3207	2134	4	0.997	2587.4 ± 56.4	KNSTD	116.9 ± 2.6	181.0 ± 6.9	124.4 ± 3.0
BCTA06-7	38.2378	-119.3161	2112	4	0.999	2664.4 ± 57.5	KNSTD	122.1 ± 2.7	195.1 ± 7.8	130.4 ± 3.1
BCTA06-8	38.2379	-119.3145	2110	2	0.999	2982.9 ± 60.8	KNSTD	135.1 ± 2.9	235.6 ± 10.2	145.3 ± 3.3
BCTA06-9	38.2380	-119.3143	2113	3	0.999	3016.1 ± 46.6	KNSTD	137.5 ± 2.2	244.4 ± 8.3	148.2 ± 2.6
Sonora Junction Tenaya moraine										
SJTE06-1	38.3258	-119.4722	2219	2	0.990	540.6 ± 10.7	KNSTD	22.3 ± 0.4	23.6 ± 0.5	22.5 ± 0.5
SJTE06-2	38.3259	-119.4723	2298	1.5	0.995	458.5 ± 10.8	KNSTD	17.7 ± 0.4	18.6 ± 0.5	17.9 ± 0.4
SJTE06-3	38.3259	-119.4726	2291	3	0.995	572.5 ± 13.4	KNSTD	22.6 ± 0.5	24.0 ± 0.6	22.8 ± 0.5
SJTE06-4	38.3259	-119.4728	2301	3	0.995	424.0 ± 10.0	KNSTD	16.6 ± 0.4	17.3 ± 0.4	16.7 ± 0.4
SJTE06-5	38.3260	-119.4729	2300	3	0.995	535.0 ± 12.5	KNSTD	20.9 ± 0.5	22.2 ± 0.6	21.2 ± 0.5
SJTE06-6	38.3253	-119.4707	2286	3	0.995	433.9 ± 10.2	KNSTD	17.1 ± 0.4	17.9 ± 0.4	17.3 ± 0.4
SJTE06-7	38.3254	-119.4706	2268	2	0.995	494.1 ± 9.6	KNSTD	19.6 ± 0.4	20.7 ± 0.4	19.8 ± 0.4
SJTE06-8	38.3253	-119.4705	2276	2	0.995	85.1 ± 3.6	KNSTD	3.3 ± 0.1	3.4 ± 0.1	3.3 ± 0.1
SJTE06-9	38.3253	-119.4705	2276	5	0.997	589.6 ± 13.8	KNSTD	23.8 ± 0.6	25.4 ± 0.6	24.1 ± 0.6
Sonora Junction Tahoe moraine										
SJTA06-1	38.3165	-119.4591	2236	3	0.994	2469.1 ± 68.7	KNSTD	103.1 ± 2.9	148.2 ± 6.5	108.9 ± 3.3
SJTA06-2	38.3166	-119.4594	2294	2	0.999	2168.4 ± 50.5	KNSTD	85.6 ± 2.0	113.5 ± 3.7	89.6 ± 2.2
SJTA06-3	38.3163	-119.4605	2307	1	0.999	2767.5 ± 65.7	KNSTD	108.1 ± 2.6	159.5 ± 6.2	114.5 ± 3.0
SJTA06-4	38.3164	-119.4604	2317	3	0.983	2159.9 ± 50.1	KNSTD	86.0 ± 2.0	114.2 ± 3.7	90.0 ± 2.2
SJTA06-5	38.3165	-119.4610	2313	3	0.999	2206.8 ± 48.4	KNSTD	86.8 ± 1.9	115.7 ± 3.6	90.9 ± 2.1
SJTA06-6	38.3165	-119.4614	2314	5	0.999	1245.3 ± 29.1	KNSTD	49.3 ± 1.2	57.0 ± 1.6	50.6 ± 1.2
SJTA06-7	38.3166	-119.4620	2310	3	0.993	1284.1 ± 23.3	KNSTD	50.5 ± 0.9	58.5 ± 1.3	51.8 ± 1.0
SJTA06-8	38.3168	-119.4625	2311	1	0.997	1937.4 ± 56.7	KNSTD	75.0 ± 2.2	95.1 ± 3.7	78.0 ± 2.4
SJTA06-9	38.3168	-119.4628	2331	3	0.999	1157.9 ± 22.1	KNSTD	44.5 ± 0.9	50.7 ± 1.1	45.6 ± 0.9
SJTA06-10	38.3169	-119.4636	2313	2	0.999	1414.9 ± 36.8	KNSTD	54.8 ± 1.4	64.4 ± 2.0	56.3 ± 1.5
Sonora Junction Tioga moraine (northern lobe)										
SJTIR06-1	38.3540	-119.4685	2108	2	0.992	431.7 ± 11.1	KNSTD	19.1 ± 0.5	20.1 ± 0.5	19.2 ± 0.5
SJTIR06-2	38.3540	-119.4685	2108	3	0.991	428.4 ± 10.4	KNSTD	19.1 ± 0.5	20.1 ± 0.5	19.3 ± 0.5
SJTIR06-3	38.3535	-119.4673	2110	4	0.992	438.4 ± 10.6	KNSTD	19.7 ± 0.5	20.7 ± 0.5	19.9 ± 0.5

SJTIR06-4	38.3535	-119.4674	2113	4	0.992	427.7 ± 10.4	KNSTD	19.1 ± 0.5	20.2 ± 0.5	19.3 ± 0.5
SJTIR06-5	38.3535	-119.4676	2113	2	0.992	425.5 ± 10.3	KNSTD	18.7 ± 0.5	19.7 ± 0.5	18.9 ± 0.5
SJTIR06-6	38.3533	-119.4669	2108	2	0.997	440.3 ± 12.9	KNSTD	19.4 ± 0.6	20.4 ± 0.6	19.5 ± 0.6
Virginia Creek Tahoe moraine										
VCTA06-1	38.0534	-119.2297	2940	2	0.996	2276.4 ± 38.7	07KNSTD	66.7 ± 1.2	82.0 ± 1.8	69.0 ± 1.2
VCTA06-2	38.0534	-119.2297	2940	1	0.996	4710.2 ± 80.3	07KNSTD	139.3 ± 2.5	252.7 ± 9.7	150.3 ± 2.9
VCTA06-3	38.0534	-119.2297	2940	3	0.996	804.4 ± 13.6	07KNSTD	23.5 ± 0.4	25.1 ± 0.5	23.8 ± 0.4
VCTA06-5	38.0534	-119.2297	2940	3	0.996	783.4 ± 13.3	07KNSTD	22.9 ± 0.4	24.4 ± 0.4	23.1 ± 0.4
VCTA06-6	38.0534	-119.2297	2940	1	0.995	2072.8 ± 35.2	07KNSTD	60.2 ± 1.0	72.2 ± 1.5	62.1 ± 1.1
VCTA06-7	38.0534	-119.2297	2940	2	0.998	1095.6 ± 22.2	07KNSTD	31.7 ± 0.6	34.7 ± 0.8	32.3 ± 0.7
VCTA06-8	38.0534	-119.2297	2940	3	0.998	1429.3 ± 24.2	07KNSTD	41.9 ± 0.7	47.2 ± 0.9	42.8 ± 0.7
VCTA06-9	38.0534	-119.2297	2940	3	0.998	800.5 ± 13.6	07KNSTD	23.3 ± 0.4	24.9 ± 0.5	23.6 ± 0.4
Lundy Canyon Tioga outwash terrace										
LCTIO-07-1	38.0293	-119.1797	2215	5	0.986	357.1 ± 8.5	07KNSTD	16.9 ± 0.4	17.7 ± 0.4	17.0 ± 0.4
LCTIO-07-2	38.0293	-119.1795	2237	4	0.985	288.8 ± 8.3	07KNSTD	13.4 ± 0.4	13.8 ± 0.4	13.4 ± 0.4
LCTIO-07-3	38.0294	-119.1791	2235	3	0.986	377.1 ± 8.9	07KNSTD	17.3 ± 0.4	18.1 ± 0.5	17.5 ± 0.4
LCTIO-07-4	38.0299	-119.1752	2206	3	0.990	385.7 ± 10.4	07KNSTD	18.0 ± 0.5	18.9 ± 0.5	18.1 ± 0.5
LCTIO-07-5	38.0301	-119.1759	2207	4	0.994	385.3 ± 10.3	07KNSTD	18.0 ± 0.5	18.9 ± 0.5	18.2 ± 0.5
LCTIO-07-6	38.0300	-119.1761	2205	5	0.994	367.1 ± 8.7	07KNSTD	17.3 ± 0.4	18.2 ± 0.5	17.5 ± 0.4
Buckeye Creek Tioga outwash terrace										
BCTI07-1	38.2359	-119.3149	2043	5	0.994	368.9 ± 8.8	07KNSTD	19.3 ± 0.5	20.4 ± 0.5	19.5 ± 0.5
BCTI07-2	38.2358	-119.3150	2052	3	0.990	403.4 ± 7.6	07KNSTD	20.7 ± 0.4	21.9 ± 0.4	21.0 ± 0.4
BCTI07-3	38.2356	-119.3153	2070	5	0.990	155.6 ± 3.2	07KNSTD	8.0 ± 0.2	8.2 ± 0.2	8.0 ± 0.2
BCTI07-4	38.2351	-119.3129	2000	5	0.990	366.1 ± 8.9	07KNSTD	19.8 ± 0.5	20.9 ± 0.5	20.0 ± 0.5
BCTI07-5	38.2351	-119.3129	2065	3	0.990	378.2 ± 9.1	07KNSTD	19.3 ± 0.5	20.3 ± 0.5	19.5 ± 0.5
BCTI07-6	38.2351	-119.3129	2070	5	0.990	267.1 ± 6.5	07KNSTD	13.8 ± 0.3	14.3 ± 0.4	13.9 ± 0.3
Lundy Canyon Mono Basin moraine										
LCMB07-1	38.0248	-119.1846	2505	5	1.000	1085.0 ± 26.2	07KNSTD	42.2 ± 1.0	47.7 ± 1.3	43.1 ± 1.1
LCMB07-2	38.0248	-119.1846	2494	4	1.000	1149.9 ± 27.8	07KNSTD	44.7 ± 1.1	50.9 ± 1.4	45.8 ± 1.1
LCMB07-3	38.0248	-119.1846	2475	4	1.000	720.6 ± 40.3	07KNSTD	28.2 ± 1.6	30.5 ± 1.9	28.7 ± 1.6
LCMB07-4	38.0248	-119.1846	2475	5	1.000	562.5 ± 15.1	07KNSTD	22.2 ± 0.6	23.6 ± 0.7	22.4 ± 0.6
LCMB07-5	38.0248	-119.1846	2440	5	1.000	888.9 ± 21.5	07KNSTD	36.0 ± 0.9	39.8 ± 1.1	36.7 ± 0.9
LCMB07-6	38.0248	-119.1846	2427	5	1.000	932.9 ± 37.7	07KNSTD	38.1 ± 1.6	42.5 ± 1.9	38.9 ± 1.6
Green Creek Tahoe moraine										
GCTA07-1	38.1301	-119.2456	2584	3	0.977	598.0 ± 14.0	07KNSTD	22.1 ± 0.5	23.5 ± 0.6	22.3 ± 0.5
GCTA07-2	38.1295	-119.2465	2607	3	0.993	571.5 ± 13.4	07KNSTD	20.5 ± 0.5	21.7 ± 0.5	20.7 ± 0.5
GCTA07-3	38.1284	-119.2493	2609	2	1.000	751.4 ± 17.5	07KNSTD	26.5 ± 0.6	28.5 ± 0.7	26.9 ± 0.6
GCTA07-4	38.1264	-119.2538	2640	1	1.000	2147.8 ± 40.8	07KNSTD	74.7 ± 1.4	94.7 ± 2.4	77.6 ± 1.6
GCTA07-5	38.1254	-119.2560	2653	3	1.000	4805.2 ± 92.6	07KNSTD	172.7 ± 3.5	469.1 ± 46.3	190.2 ± 4.3
GCTA07-6	38.1254	-119.2554	2645	3	1.000	1064.9 ± 20.3	07KNSTD	37.2 ± 0.7	41.3 ± 0.9	37.9 ± 0.7
Lundy Canyon Tioga moraine										
LCTI07-1	38.0273	-119.1785	2324	5	0.994	365.9 ± 8.7	07KNSTD	16.0 ± 0.4	16.7 ± 0.4	16.1 ± 0.4
LCTI07-2	38.0272	-119.1785	2314	1	0.994	416.2 ± 9.8	07KNSTD	17.7 ± 0.4	18.6 ± 0.5	17.9 ± 0.4
LCTI07-3	38.0272	-119.1785	2314	3	0.994	376.9 ± 7.5	07KNSTD	16.3 ± 0.3	17.0 ± 0.4	16.4 ± 0.3
LCTI07-4	38.0270	-119.1763	2290	5	0.994	438.8 ± 10.4	07KNSTD	19.6 ± 0.5	20.7 ± 0.5	19.8 ± 0.5
LCTI07-5	38.0269	-119.1761	2283	4	0.994	426.3 ± 10.1	07KNSTD	19.0 ± 0.5	20.0 ± 0.5	19.2 ± 0.5
LCTI07-6	38.0270	-119.1759	2285	5	0.994	320.0 ± 6.2	07KNSTD	14.3 ± 0.3	14.9 ± 0.3	14.4 ± 0.3
Sonora Junction Tahoe outwash terrace depth profile										
SJPT06-2	38.3820	-119.4408	2260	*40*	0.999	807.3 ± 18.9	07KNSTD	n/a	n/a	n/a
SJPT06-3	38.3820	-119.4408	2260	*60*	0.999	996.7 ± 23.6	07KNSTD	n/a	n/a	n/a
SJPT06-4	38.3820	-119.4408	2260	*80*	0.999	1006.1 ± 23.4	07KNSTD	n/a	n/a	n/a
SJPT06-5	38.3820	-119.4408	2260	*100*	0.999	843.0 ± 20.0	07KNSTD	n/a	n/a	n/a
SJPT06-6	38.3820	-119.4408	2260	*120*	0.999	695.9 ± 16.4	07KNSTD	n/a	n/a	n/a
SJPT06-7	38.3820	-119.4408	2260	*140*	0.999	537.9 ± 12.7	07KNSTD	n/a	n/a	n/a
SJPT06-8	38.3820	-119.4408	2260	*160*	0.999	394.7 ± 9.8	07KNSTD	n/a	n/a	n/a
SJPT06-9	38.3820	-119.4408	2260	*180*	0.999	370.5 ± 7.1	07KNSTD	n/a	n/a	n/a
SJPT06-10	38.3820	-119.4408	2260	*200*	0.999	284.3 ± 8.9	07KNSTD	n/a	n/a	n/a
SJPT06-11	38.3820	-119.4408	2260	*220*	0.999	251.3 ± 5.9	07KNSTD	n/a	n/a	n/a
SJPT06-12	38.3820	-119.4408	2260	*240*	0.999	226.2 ± 5.6	07KNSTD	n/a	n/a	n/a
SJPT06-13	38.3820	-119.4408	2260	*260*	0.999	203.4 ± 4.8	07KNSTD	n/a	n/a	n/a

Table 1 (*continued*)

Sample name	Latitude (DD)	Longitude (DD)	Elevation (m)	Thickness (cm) or *depth (cm)*	Shielding correction[a]	$[^{10}Be]$ (10^3 atoms g^{-1})[b]	Standard	Minimum exposure age (ky)[c] erosion rate: 0	Maximum exposure age (ky)[d] erosion rate: 3.1 m/Myr	Preferred exposure age (ky)[e] erosion rate: 0.6 m/Myr
SJPT06-14	38.3820	-119.4408	2260	*280*	0.999	218.4 ± 6.3	07KNSTD	n/a	n/a	n/a
Lundy Canyon Sherwin moraine										
LCSH07-1	38.0208	-119.1848	2561	3	0.991	1091.0 ± 20.8	07KNSTD	40.6 ± 0.8	45.6 ± 1.0	41.5 ± 0.8
LCSH07-2	38.0204	-119.1845	2567	2	0.971	2248.8 ± 52.2	07KNSTD	85.4 ± 2.0	113.1 ± 3.7	89.3 ± 2.2
LCSH07-3	38.0206	-119.1843	2560	3	0.991	1373.2 ± 29.4	07KNSTD	51.3 ± 1.1	59.7 ± 1.5	52.7 ± 1.2
LCSH07-4	38.0214	-119.1820	2516	2	0.991	1173.3 ± 33.4	07KNSTD	44.6 ± 1.3	50.8 ± 1.7	45.7 ± 1.3
LCSH07-5	38.0220	-119.1802	2480	3	0.991	1871.3 ± 43.4	07KNSTD	74.0 ± 1.8	93.5 ± 2.9	76.9 ± 1.9
LCSH07-6	38.0217	-119.1801	2480	5	0.991	2376.9 ± 53.1	07KNSTD	96.1 ± 2.2	133.6 ± 4.5	101.1 ± 2.4
Woodfords Tioga outwash terrace										
WFTI08-1	38.7759	-119.8199	1691	3	0.994	299.4 ± 7.2	07KNSTD	19.4 ± 0.5	20.4 ± 0.5	19.6 ± 0.5
WFTI08-2	38.7746	-119.8210	1712	2	0.993	322.4 ± 7.9	07KNSTD	20.5 ± 0.5	21.6 ± 0.6	20.7 ± 0.5
WFTI08-3	38.7746	-119.8212	1713	5	0.993	332.0 ± 7.9	07KNSTD	21.6 ± 0.5	22.9 ± 0.6	21.8 ± 0.5
Woodfords Tahoe outwash terrace										
WFTA08-1	38.7721	-119.8171	1663	4	0.985	1773.8 ± 31.7	07KNSTD	122.5 ± 2.3	195.5 ± 6.4	130.8 ± 2.6
WFTA08-2	38.7724	-119.8158	1725	3	0.991	1789.5 ± 26.6	07KNSTD	116.4 ± 1.8	179.5 ± 4.7	123.9 ± 2.0
WFTA08-3	38.7710	-119.8216	1789	3	0.995	1100.9 ± 21.1	07KNSTD	67.4 ± 1.3	82.9 ± 2.0	69.8 ± 1.4

[a] Ratio of the production rate at the shielded site to that for a 2π surface at the same location calculated using the CRONUS-Earth Geometric Shielding Calculator Version 1.1.
[b] Calculated using KNSTD or 07KNSTD ^{10}Be measurement standard and calibration (Nishizumi et al., 2007).
[c] Model exposure age assuming no inheritance, zero erosion, density 2.7 g/cm^3, and standard atmosphere calculated using the CRONUS-Earth ^{10}Be – ^{26}Al exposure age calculator (Balco et al., 2008) Version 2.2 using a constant production rate model and scaling scheme for spallation after Lal (1991) / Stone (2000). This version of the CRONUS calculator (constants: 2.2-dev) uses a reference spallogenic ^{10}Be production rate of 4.49 ± 0.39 atoms g^{-1} yr^{-1} (± 1σ, SLHL) and muonogenic production after Heisinger et al. (2002a, b). The quoted uncertainty is the 1σ internal error, which reflects measurement uncertainty only.
[d] Exposure age calculated using the same method, except using an erosion rate of 3.1 m/Myr (Small et al., 1997).
[e] Exposure age calculated using the same method, except using an erosion rate of 0.6 m/Myr.

1967) were sampled along crests of the right-lateral and terminal moraine complexes of two different ice lobes (Fig. 2). Using the method of Anderson et al. (1996), an outwash surface (Tahoe outwash of Clark, 1967) directly outside of and graded to the Tahoe moraines was sampled using a depth profile collected ~4 km NNE of Sonora Junction.

3.1.1. High confidence age estimates (P > 0.05)

3.1.1.1. Boulder ages. A χ^2_R value near 1 and high P is interpreted to indicate that the spread of the ^{10}Be concentrations is well described by the analytical uncertainty, which implies that geologic uncertainties are minimal (i.e., moraine-crest stabilization was rapid and pre- or post-depositional processes are insignificant). In this case, we take the unweighted arithmetic mean and 1σ standard deviation as the best-estimate of true depositional age with relatively high confidence. High confidence deposits include: the Sonora Junction Tioga moraines, Lundy Canyon Tioga outwash terrace, Buckeye Creek Tahoe outwash terrace, Sonora Junction Tahoe outwash terrace, Soda Springs Tioga moraine (Amos et al., 2010), Bloody Canyon Tioga 3 moraine (Schaefer et al., 2006), Bear Valley early Tioga moraine (James et al., 2002), Bishop Creek Tioga 3 moraine (Phillips et al., 2009), Bishop Creek Tahoe 1 moraine (Phillips et al., 2009), and Bishop Creek Tahoe 2 moraine (Phillips et al., 2009).

Ages from the outermost Tioga moraine of the northern lobe at Sonora Junction (SJTIR06-, Table 1) range from 19 to 20 ka. All the data ($n = 6$) cluster tightly (Fig. 3A) with a mean age of 19.4 ± 0.3 ka. A χ^2_R value of 0.4 and P equal to 0.82 for this dataset indicates that the scatter can be explained by analytical uncertainty alone (Table 2). The outermost Tioga moraine of the southern lobe at Sonora Junction (SJTI05-, Table 1) yields ages ranging from 16 to 22 ka, of which the two oldest and one youngest age are considered outliers (Fig. 3B). The remaining data ($n = 6$: Table 2) define a peak with a mean age of 19.2 ± 0.6 ka ($\chi^2_R = 1.4$, $P = 0.21$).

3.1.1.2. Depth profile. Thirteen samples were analyzed from a 3-m-deep depth profile on the Tahoe outwash terrace at Sonora Junction (SJPT06, Table 1). The overall exponential decrease in ^{10}Be concentration with depth (Fig. 4) suggests that the terrace is a single depositional unit. The shallowest two samples (at 40 and 60 cm) are omitted from the fit as outliers that probably resulted from bioturbation in the soil A-horizon (Perg et al., 2001). Nine samples from 0.8 to 2.4 m depth are well described by a best-fit exponential function using an effective attenuation length for production by high-energy spallation of 160 g/cm^2 (Gosse and Phillips, 2001), sediment density of 2 g/cm^3, and an inheritance value of 8.8×10^4 atoms gram^{-1} (~3% of the surface concentration). This non-linear function was fit to the data by minimizing the sum of the squares of the errors between the measured ^{10}Be concentrations and predicted values, and, in turn, the best-fit result was solved for the surface concentration. The preferred exposure age uses an erosion rate of 3.1 m/Myr, similar to weathered boulder and bedrock erosion rates (discussed further in Section 4.1.1). The lack of a thick soil Av horizon suggests insignificant inflation of the terrace surface. We did not measure the sediment density in the field, and thus assume a density of 2 g cm^{-3} based on measurements in similar sediments in published studies, e.g., Kirby et al. (2006). The deepest two samples (at 260 and 280 cm) do not fit the single exponential function and are omitted from the fit because they suggest a significant contribution from production by muons that were not considered in the fit calculations. Results give a best-fit age (corrected for inheritance) of 149 ± 11 ka.

3.1.2. Moderate confidence age estimates (P < 0.05)

A group of samples with a moderate χ^2_R value and $P < 0.05$ indicates that the scatter is not explained by analytical uncertainties alone, such that an additional source of uncertainty is

Table 2
Summary statistics and best-estimate or minimum surface exposure ages for Sierra Nevada glacial deposits

| Mean age (ky)[a]	n	Reduced χ2	P	Oldest age (ky)[a]	Best-estimate depositional age (ky)[a]	Confidence	Minimum age (ky)[a]	Reference	Figure
[10]Be									
Robinson Creek Tahoe moraine (RCTA05)									
121.4 ± 7.8	5	4.9	< 0.01	152.5 ± 2.6	152.5 ± 2.6	low	n/a	this study	S4
Sonora Junction Tioga moraine (southern lobe) (SJTI05)									
19.2 ± 0.6	6	1.4	0.21	22.0 ± 0.6	19.2 ± 0.6	high	n/a	this study	3B
Buckeye Creek Tahoe outwash terrace (BCTA06)									
148.3 ± 2.2	4	0.5	0.72	167.4 ± 4.4	148.3 ± 2.2	high	n/a	this study	S2
Sonora Junction Tenaya moraine (SJTE06)									
20.3 ± 2.8	8	37	< 0.01	24.1 ± 0.6	20.3 ± 2.8	moderate	n/a	this study	3C
Sonora Junction Tahoe moraine (SJTA06)									
77.6 ± 25.1	10	332	< 0.01	114.5 ± 3.0	n/a	low	114.5 ± 3.0	this study	3D
Sonora Junction Tioga moraine (northern lobe) (SJTIR06)									
19.4 ± 0.3	6	0.4	0.82	19.9 ± 1.0	19.4 ± 0.3	high	n/a	this study	3A
Virginia Creek Tahoe moraine (VCTA06)									
53.4 ± 43.0	8	2750	< 0.01	150.3 ± 2.9	150.3 ± 2.9	low	n/a	this study	S8
Lundy Canyon Tioga outwash terrace (LCTIO-07)									
17.7 ± 1.0	5	1.2	0.29	18.2 ± 1.0	17.7 ± 1.0	high	n/a	this study	S13
Buckeye Creek Tioga outwash terrace (BCTI07)									
20.0 ± 0.7	4	2.8	0.04	21.0 ± 1.0	20.0 ± 0.7	moderate	n/a	this study	S3
Lundy Canyon Mono Basin moraine (LCMB07)									
41.1 ± 4.1	4	15	< 0.01	45.8 ± 1.1	45.8 ± 1.1	low	n/a	this study	S11
Green Creek Tahoe moraine (GCTA07)									
62.6 ± 66.0	6	3850	< 0.01	190.2 ± 4.3	190.2 ± 4.3	low	n/a	this study	S6
Lundy Canyon Tioga moraine (LCTI07)									
17.9 ± 1.6	5	16	< 0.01	19.8 ± 1.0	17.9 ± 1.6	moderate	n/a	this study	S12
Sonora Junction Tahoe outwash terrace depth profile (SJPT06)									
n/a	9	n/a	n/a	n/a	149.1 ± 10.5	high	n/a	this study	4
Lundy Canyon Sherwin moraine (LCSH07)									
67.9 ± 24.8	6	369	< 0.01	101.1 ± 2.4	n/a	low	101.1 ± 2.4	this study	S10
Woodfords Tioga outwash terrace (WFTI08)									
20.7 ± 1.1	3	4.8	< 0.01	21.8 ± 0.5	20.7 ± 1.1	moderate	n/a	this study	S16
Woodfords Tahoe outwash terrace (WFTA08)									
108.2 ± 33.4	3	444	< 0.01	130.8 ± 2.6	n/a	low	130.8 ± 2.6	this study	S15
Soda Springs Tioga moraine									
18.3 ± 1.0	5	1.3	0.26	19.0 ± 1.0	18.3 ± 1.0	high	n/a	Amos et al. (2010)	S20
Whitney Portal Tioga moraine									
18.9 ± 1.1	6	4.7	< 0.01	20.2 ± 0.9	18.9 ± 1.1	moderate	n/a	Benn et al. (2006)	S18
Bear Valley early Tioga moraine									
20.5 ± 1.8	2	1.4	0.23	21.8 ± 1.6	20.5 ± 1.8	high	n/a	James et al. (2002)	S17
Bloody Canyon Tioga 3 moraine									
18.4 ± 1.6	4	1.7	0.16	20.5 ± 1.3	18.4 ± 1.6	high	n/a	Schaefer et al. (2006)	S19
[36]Cl									
Bishop Creek Tahoe 1 moraine									
143.6 ± 7.5	6	1.9	0.09	168.5 ± 5.8	143.6 ± 7.5	high	n/a	Phillips et al. (2009)	S21
Bishop Creek Tahoe 2 moraine									
134.4 ± 6.5	10	1.5	0.14	145.2 ± 6.3	134.4 ± 6.5	high	n/a	Phillips et al. (2009)	S22
Bishop Creek Tahoe 3 moraine									
100.2 ± 6.6	6	2.7	0.02	127.4 ± 4.3	100.2 ± 6.6	moderate	n/a	Phillips et al. (2009)	S23
Bishop Creek Tahoe 4 moraine									
91.7 ± 22.1	22	75	< 0.01	131.0 ± 4.3	n/a	low	131.0 ± 4.3	Phillips et al. (2009)	S24
Bishop Creek Tahoe 5 moraine									
81.4 ± 44.2	3	225	< 0.01	132.3 ± 4.6	n/a	low	132.3 ± 4.6	Phillips et al. (2009)	S25
Bishop Creek Tahoe 6 moraine									
96.7 ± 40.1	5	854	< 0.01	129.3 ± 4.2	n/a	low	129.3 ± 4.2	Phillips et al. (2009)	S26
Bishop Creek Tioga 1 moraine									
22.2 ± 1.7	6	5	< 0.01	32.9 ± 1.2	22.2 ± 1.7	moderate	n/a	Phillips et al. (2009)	S27
Bishop Creek Tioga 3 moraine									
18.5 ± 0.8	11	1.6	0.09	20.0 ± 0.6	18.5 ± 0.8	high	n/a	Phillips et al. (2009)	S28
Bishop Creek Tioga 4 moraine									
15.4 ± 1.1	25	4.6	< 0.01	22.4 ± 0.7	15.4 ± 1.1	low	n/a	Phillips et al. (2009)	S29

[a] The quoted uncertainty is the 1σ error. See text for details.

present in the dataset, e.g., erosion, inheritance, spalling, tumbling, exhumation. If the scatter is moderate, then the geologic uncertainty may be relatively minor. For example, if the 0.05 > P > 0.01 or the mean and standard deviation of the group overlaps with the oldest age within error, then we take the mean and standard deviation of ages to describe the best-estimate depositional age with moderate confidence. Moderate confidence age estimates include: the Buckeye Creek Tioga outwash terrace, Sonora Junction

Tenaya moraine, Lundy Canyon Tioga moraine, Woodfords Tioga moraine, Whitney Portal Tioga moraine (Benn et al., 2006), Bishop Creek Tioga 1 moraine (Phillips et al., 2009), and Bishop Creek Tahoe 3 moraine from Phillips et al. (2009).

The 9 ages from the Tenaya moraine at Sonora Junction (SJTE6-, Table 1) are scattered between 3 and 24 ka. Even omitting the youngest age does not create a clear peak in the remaining age distribution (Fig. 3C). The mean age for these samples (n = 8) is
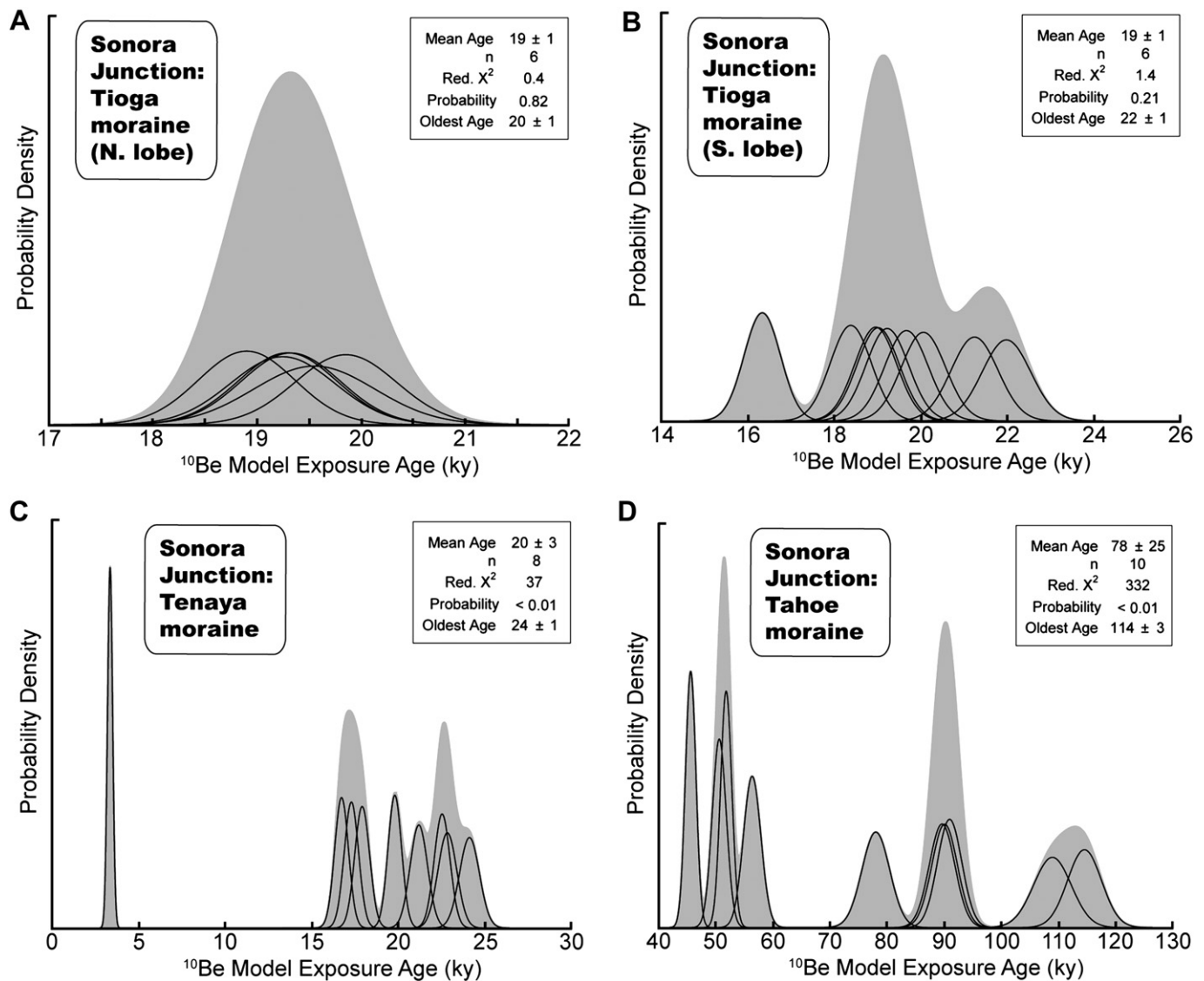
Fig. 3. A) Probability density function for ^{10}Be boulder ages from the Sonora Junction Tioga moraine (northern lobe) (SJTIR06) with summary statistics. Black curves are individual sample PDFs defined by the age and 1σ analytical error. A cumulative probability density function (grey curve) is calculated by summing individual PDFs for all boulders from each deposit. B) Probability density function and summary statistics for ^{10}Be boulder ages from the Sonora Junction Tioga moraine (southern lobe) (SJTI05). C) Probability density function and summary statistics for boulder ^{10}Be ages from the Sonora Junction Tenaya moraine (SJTE06). D) Probability density function and summary statistics for ^{10}Be boulder ages from the Sonora Junction Tahoe moraine (SJTA06).

20.3 ± 2.8 ka ($\chi_R^2 = 37$, $P < 0.01$). Regardless of the high χ_R^2 value, the average and the oldest age of 24.1 ± 0.6 ka overlap within error. Hence, we use the average of 20.3 ± 2.8 ka to estimate the depositional age.

3.1.3. Low confidence age estimates (P << 0.01)

Some deposits have a large range of ages that results in a very high χ_R^2 value and very low P (<<0.01). These data are interpreted to indicate poor preservation that results in highly uncertain ages for these deposits. Relying on results of numerical models, we interpret the oldest age in a distribution to best-estimate the true depositional age (Putkonen and Swanson, 2003; Putkonen and O'Neal, 2006) because post-depositional processes can lead to erroneously young ages. For these deposits, the oldest age with its analytical uncertainty is quoted as the depositional age. In some extreme cases, the oldest apparent age is considered a minimum depositional age. Low confidence age results include: the Green Creek Tahoe moraine, Lundy Canyon Mono Basin moraine, Lundy Canyon Sherwin moraine, Robinson Creek Tahoe moraine, Sonora Junction Tahoe moraine, Virginia Creek Tahoe moraine, Woodfords

Tahoe outwash terrace, Bishop Creek Tahoe 4 moraine (Phillips et al., 2009), Bishop Creek Tahoe 5 moraine (Phillips et al., 2009), Bishop Creek Tahoe 6 moraine (Phillips et al., 2009), and Bishop Creek Tioga 4 moraine (Phillips et al., 2009). Low confidence ages occur mostly in older moraines where geologic uncertainty has the time to become significant.

The Tahoe moraine at Sonora Junction (SJTA06-, Table 1) has a scattered age distribution ranging from 51 to 115 ka with no clear peak in the cumulative PDF (Fig. 3D). A simple arithmetic mean of the entire dataset ($n = 10$) gives a mean age of 78 ± 25 ka. Due to the high χ_R^2 value (332) and low P (<0.01), the oldest age of 115 ± 3 ka is taken as a minimum depositional age.

3.2. Timing of Sierra Nevada glaciations

The dated LGM deposits in the Sierra Nevada of either the high and moderate confidence age results ($\chi_R^2 = 1.0$; $P = 0.43$; $n = 13$) or only high confidence results ($\chi_R^2 = 1.1$; $P = 0.38$; $n = 7$) give arithmetic mean ages of 19.4 ± 2.6 and 18.8 ± 1.9 (2σ), respectively (Fig. 5), and
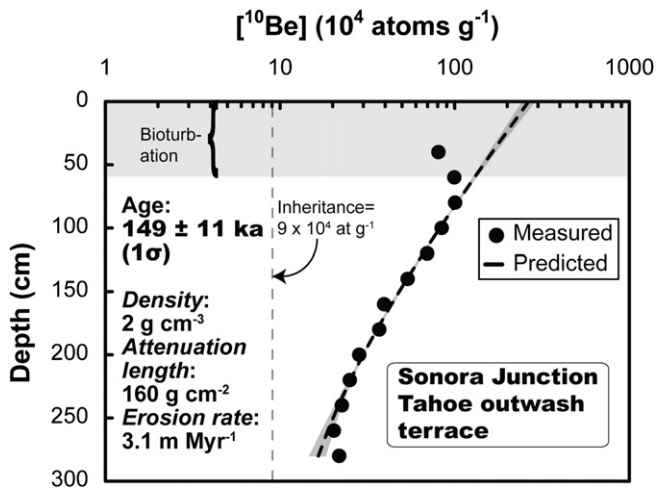
Fig. 4. Sonora Junction Tahoe outwash terrace [10]Be depth profile. Model profile calculated using an effective attenuation length for spallation of 160 g cm^{-2} (Gosse and Phillips, 2001) and sediment density of 2 g cm^{-3}. Error envelope (grey) shows range of best-fit profiles for densities from 1.8 to 2.2 g cm^{-3}. 1σ error bars on measurements are smaller than the data point symbols.

weighted averages of 19.3 ± 0.4 and 19.1 ± 0.5 (2σ) ka, respectively. The χ_R^2 values near 1 and high P indicate that the data, within the quoted errors, are consistent with a normally distributed parent population defined by the arithmetic mean and standard deviation for each group. All deposits overlap with the mean within their 2σ errors, including those dated with [10]Be and [36]Cl. When viewed from south to north (left to right, Fig. S31) and considering results from east and west of the range crest, both the consistent ages and lack of a statistically significant latitudinal spatial trend in the moderate confidence data or only high confidence data suggest a similar age for glacial retreat throughout the range at 18.8 ± 1.9 ka.

Arithmetic mean ages for penultimate glacial deposits (Fig. 6) were calculated from either both high and moderate confidence age results or only high confidence results. The moderate
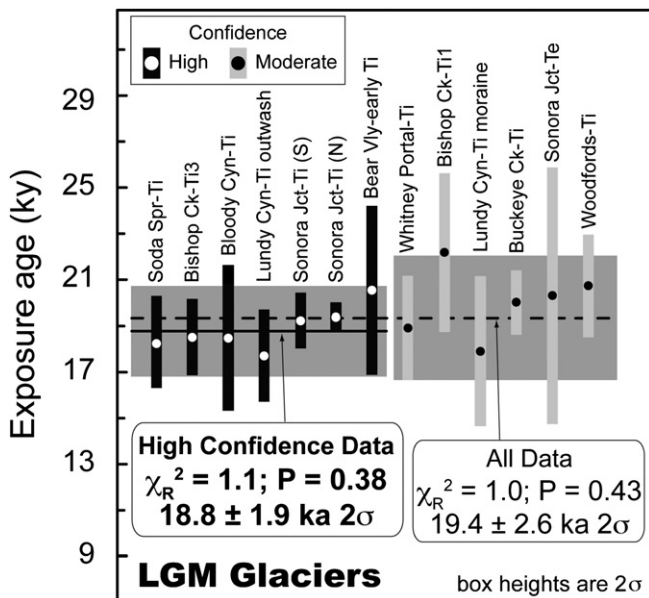
Fig. 5. Arithmetic means and statistics of dated LGM glacial deposits in the Sierra Nevada calculated from high and moderate confidence age results. Sites are organized from south to north (left to right) within each confidence group. Solid black horizontal line is mean of high confidence data. Dashed black horizontal line is mean of all data. Note that data include results from east and west of the range crest and from [10]Be and [36]Cl.
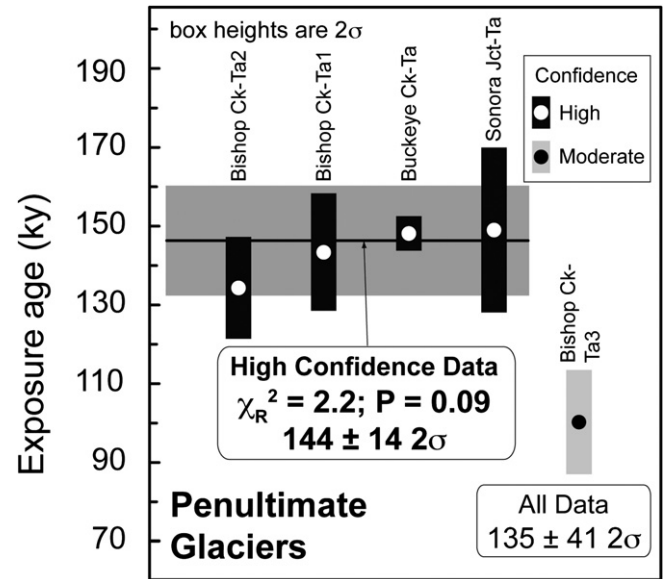
Fig. 6. Arithmetic means and statistics of dated penultimate glacial deposits in the Sierra Nevada calculated from high and moderate confidence age results. High confidence sites are organized from south to north (left to right). Solid black horizontal line is mean of high confidence data. Note that data include results from east and west of the range crest and from [10]Be and [36]Cl.

confidence site at Bishop Creek (BI-Ta3) is considered an outlier because its age does not overlap the mean of all sites ($n = 5$) at the 2σ level. However, the four high confidence sites overlap within 2σ error of the mean ($\chi_R^2 = 2.2$; $P = 0.09$; $n = 4$). Results for deposits dated with [10]Be match those from [36]Cl within 2σ error. These data indicate glacial retreat at 144 ± 14 ka (2σ).

4. Discussion

4.1. Surface exposure dating

4.1.1. Uncertainties in [10]Be ages

The accuracy of surface exposure ages is limited by uncertainties in geologic processes, e.g., inheritance and erosion, and cosmogenic nuclide production parameters. The assumption of zero inheritance in glacial deposits is supported by recent [10]Be measurements on historic moraines, which indicate <100 years of prior exposure for many boulders in the rapidly eroding Southern Alps of New Zealand (Schaefer et al., 2009). This New Zealand example, however, has very high uplift rates, short catchments, and rapidly moving glaciers, and the assumption of zero inheritance may not be valid everywhere. The assumption of zero inheritance does seem to apply in many locations, especially in regions like New Zealand and the eastern Sierra Nevada where glaciers debouch on flat plains so that the moraine record is spread out and inter-moraine contamination is less likely. We acknowledge that inheritance is an unquantifiable uncertainty in our analysis. Variable boulder inheritance is evidenced in our data, but samples with significant inheritance are identified as outliers in PDFs and omitted from depositional age interpretations. For our high confidence deposits, inheritance does not appear to contribute significant errors to our exposure ages (Putkonen and Swanson, 2003).

Model exposure ages are also sensitive to erosion of moraine boulders. For surface boulder samples, 3.1 m/Myr is considered a reasonable maximum because it falls in the range of previous studies of erosion rates estimated from weathered boulders and bedrock exposures in the Sierra Nevada (Small et al., 1997; Nichols et al., 2006).

We expect these Sierra Nevada examples are eroding faster than our samples for which minimal surface erosion was a selection criterion. An erosion rate of 0.6 m/Myr is preferred because it allows for ∼1–1.5 cm of total boulder erosion over 18–25 ky, which is consistent with (1) geologic observations of surface roughness on some sampled boulders, and (2) previous studies of boulder erosion in the Sierra Nevada and similar environments, e.g., Bierman and Gillespie (1991), Benedict (1993), Phillips et al. (1997).

For the Sonora Junction depth profile, the preferred exposure age uses an erosion rate of 3.1 m/Myr, similar to weathered boulder and bedrock erosion rates. This rate is chosen because (1) we predict that the erosion rate for the terrace tread (composed of unconsolidated sand and gravel) is higher than the boulder erosion rate and (2) it allows for a maximum of 50 cm of total erosion of the terrace tread. Evidence for <50 cm of total erosion of the terrace tread is supported by results from a coeval outwash surface at Buckeye Creek (BCTA06-, Table 1) where cosmogenic ages scale with boulder height; boulders >50 cm tall giving consistent age results, whereas boulders <50 cm above the modern surface give anomalously young ages (Fig. S30). We interpret this age pattern to indicate that the small boulders have been exhumed from the subsurface by tread erosion not exceeding 50 cm and that this value is also an appropriate estimate for the maximum erosion of the Sonora Junction surface. The true uncertainties on the model exposure age, however, may be underestimated, because we are unable to quantify the uncertainty on the erosion rate, e.g., Hein et al. (2009).

We calculate exposure ages for samples using a range of erosion rates (Table 1). For LGM deposits, ages are insensitive to this range of erosion rates. Our preferred ages change <5% (<1 ky) when the full range of erosion rates between zero and 3.1 m/Myr is considered. This restricted change indicates that results for LGM deposits are insensitive to erosion rate uncertainties. However, ages for penultimate glacial deposits are more sensitive to this range of erosion rates. Boulder ages assuming zero erosion are <10% (<15 ky) younger than our preferred estimates. Although ages could be up to 50% (75 ky) older if the 3.1 m/My erosion rate were applied, we consider this unlikely. For example, a boulder eroding at 3.1 m/My for 150 ky would have lost ∼50 cm of rock, but we never find field evidence for this magnitude of erosion. The age calculated from the Sonora Junction depth profile could be up to 30% (36 ky) younger if erosion were zero on the surface, but our estimates of total erosion from a similarly-aged surface at Buckeye Creek (Fig. S30) makes this unlikely. Uncertainties in the erosion rate limit the accuracy of our age estimates for deposits of the penultimate glaciation. However, we consider our preferred ages for penultimate deposits as reasonable estimates.

Uncertainties in the [10]Be production parameters also limit the accuracy of our age calculations. Balco et al. (2009) suggest that samples calculated using a regionally calibrated production rate from New England could be 6–12% older than those calculated using the global reference rate. Putnam et al. (2010) make a similar argument for production rates in New Zealand. These differences in production rates are not accepted as globally applicable, but instead are currently applied only to two specific regions. At this time, however, a debate persists on whether regional variations in production rates exist or whether the widely used global production value is too high. We, therefore, use the globally calibrated values with a 5% uncertainty (Table S1; Balco et al., 2008). The global reference dataset is dominated by mid-latitude, high-elevation calibration sites, several of which are in the western US, including the Sierra Nevada, and therefore appear appropriate to our sites. Moreover, a recent calibration study in the western US (Lake Bonneville shorelines, Utah; Lifton et al., 2009) indicates a spallogenic production rate consistent with the previous global estimates used in our age calculations (Balco et al., 2008). With refinements to regional or global production rates, absolute ages

could change systematically. A 6–12% reduction in the production rate, however, would not affect our major conclusions (in fact, it would make the initial LGM retreat less correlated with the Heinrich event 1 discussed in Section 4.2.3), nor would it change relative ages or patterns in the timing of retreat.

Uncertainties also exist concerning the spatial scaling and temporal variations of the cosmic ray flux. We compare results using five different scaling schemes (Stone, 2000, after Lal, 1991; Dunai, 2001; Lifton et al., 2005; Desilets et al., 2006) (Table S1) in order to get a sense for how these uncertainties affect our age calculations. Differences among results for various schemes are <5% (<1 ky) for LGM and <15% (<25 ky) for penultimate glacial deposits. This comparison suggests that uncertainties in the scaling are only potentially significant for older (Tahoe) ages and do not affect our relative ages.

4.1.2. Comparison of [10]Be and [36]Cl chronologies

Uncertainties in the [36]Cl production parameterizations yield errors that limit the accuracy of ages and make detailed paleoclimate correlations challenging. Previous studies in the Sierra Nevada mostly used [36]Cl in whole rock samples, e.g., Phillips et al. (2009)). Production parameterization for whole rock [36]Cl ages are complicated by multiple production reactions, e.g., production of [36]Cl by low energy neutrons (Gosse and Phillips, 2001). Such complications have resulted in published [36]Cl production rate estimates that differ by up to 50% (Schimmelpfennig et al., 2009). For Sierra Nevada moraines, Phillips et al. (2009) showed that, compared to calculations using the production parameterizations of Phillips et al. (2001), ages based on Stone et al. (1996a,b) and Swanson and Caffee (2001) parameterizations are 11 ± 6% and 30 ± 6% younger, respectively. [10]Be measurements in quartz provide a method that is less sensitive to non-spallation production pathways, bulk rock chemistry, and related analytical constraints. Given the large differences in results from different [36]Cl parameterization methods, it should be easy to detect significant differences between [10]Be and [36]Cl that would suggest errors in production parameterizations.

When we compare results from age-equivalent moraines in multiple valleys, our [10]Be results are consistent with [36]Cl ages calculated using either Phillips et al. (2001) or Stone et al. (1996a, 1996b) parameterizations within error. A bias toward slightly younger ages from [36]Cl may indicate slightly overestimated [36]Cl production rates. Our [10]Be chronology appears, however, inconsistent with Swanson and Caffee (2001) and suggests that [36]Cl production rates are too high for the Swanson and Caffee (2001) parameterization.

4.1.3. Comparison of Tahoe moraine and outwash chronologies

In Patagonia, Hein et al. (2009) found that flat outwash terraces were quite stable in comparison to steep-sided moraines where degradation led to exhumation of moraine boulders. We obtain high confidence ages from an old outwash terrace, e.g., Buckeye Creek Tahoe outwash, of the penultimate glaciation and lower confidence ages from an age-equivalent moraine, e.g., Robinson Creek Tahoe moraine, which supports the suggestion that outwash surfaces are more stable and can yield more reliable ages than old moraines. However, general agreement exists between at least the oldest moraine boulders, e.g., Robinson Creek Tahoe moraine, and the majority of outwash terrace ages on the Buckeye Creek Tahoe outwash. The reasonable consistency between the Tahoe-age outwash and moraine deposits reinforces the contention that these Sierran moraines can be relatively stable over the long-term. In contrast, in Patagonia, Hein et al. (2009) found moraine boulders were apparently significantly younger (∼100 ky) than adjacent outwash where degradation of moraines was clearly playing a significant role.
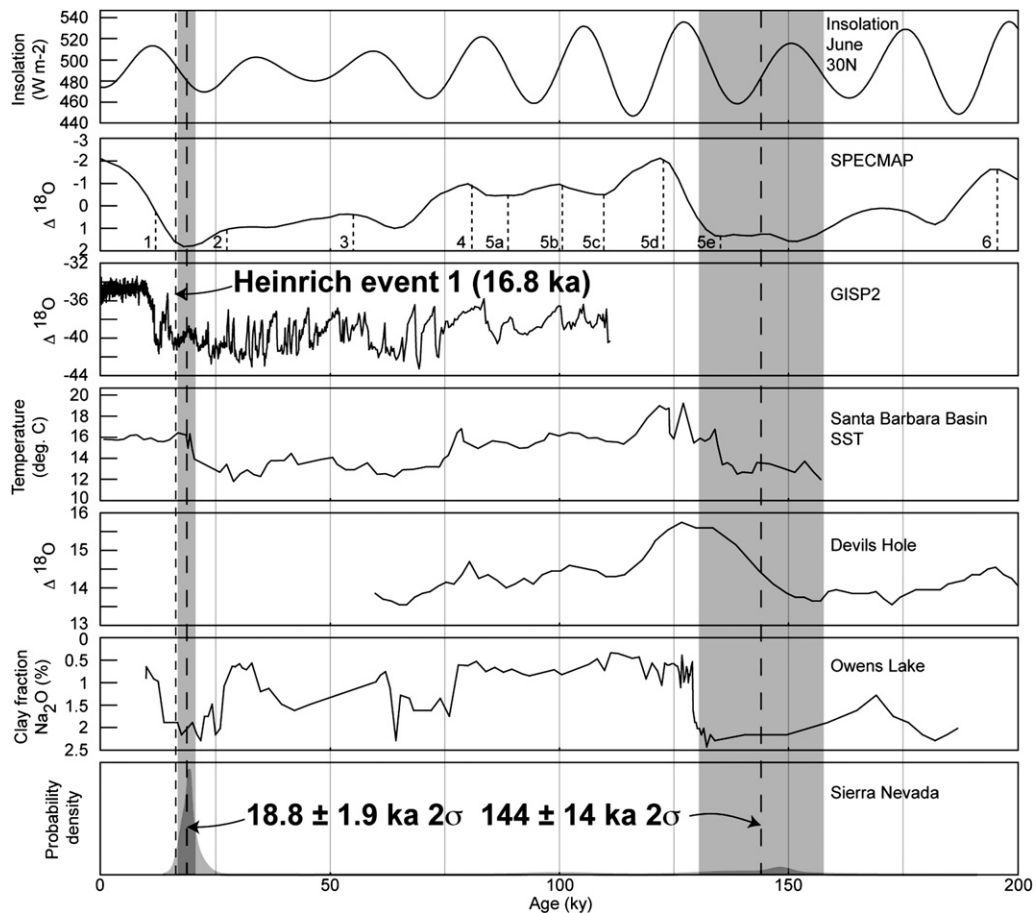
Fig. 7. Temporal relation between Sierra Nevada glacial chronology from surface exposure dating results and climate-forcing factors. Probability density function for Sierra Nevada includes all high and moderate confidence sites. Tie lines (large dashed) are arithmetic means of high confidence data with 2σ uncertainties (grey box) and Heinrich event 1 (small dashed). See section Section 4.2.1 for data sources.

4.2. Comparison to paleoclimate records

4.2.1. Regional proxy records

Our chronology shows good correlation to several regional terrestrial proxy records and marine sea-surface temperature estimates (Fig. 7). The Owens Lake record is a regional proxy in the southern Sierra Nevada for glacial rock-flour input into a lacustrine system (Bischoff et al., 1997) based on the age model of Litwin et al. (1999). Dated Sierra Nevada glacial deposits generally correspond with rock-flour maxima during both the last and penultimate glaciations (Fig. 7). Data from Devils Hole is a regional terrestrial paleotemperature record for the southwest United States (Winograd et al., 1997). Based on a comparison of our data with the Devils Hole record, the penultimate Sierra Nevada glaciation reached its maximum at the end of the coldest period of MIS 6. Santa Barbara Basin marine sediment alkenone data from ODP site 1014 give reconstructed Pacific sea-surface temperatures (Yamamoto et al., 2007). Initial LGM glacial retreat in the Sierra occurred apparently after a 10-ky-long period of rapid warming to near modern sea-surface temperature. In contrast, the penultimate glaciation appears to correlate with a prolonged Pacific sea-surface temperature minimum that occurred during MIS 6.

A significant difference between these proxy records and our glacial chronology is that we do not observe glacial deposits dating to between ∼25–140 ka. Although results for individual boulders fall within this range, the ages of the deposits within which they

occur cannot be judged with any confidence. Increased rock-flour input into Owens Lake and decreased temperatures in the Devils Hole record during this interval, especially between 65 and 80 ka (Fig. 7), would suggest the presence of Sierra Nevada glaciers during this period, but no coeval moraines or outwash surfaces were dated in this study. The lack of deposits in this age range may indicate that the moraine record is incomplete because of obliterative overlap (Gibbons et al., 1984), consistent with the results of Phillips et al. (2009).

4.2.2. Significance of patterns in western US alpine glaciation

Previous studies suggest that alpine glacier systems are more likely to be in phase with global patterns if they were (1) less affected by local effects, e.g., the anticyclonic winds of the Laurentide Ice Sheet (Licciardi and Pierce, 2008) (2) more directly connected to the constant moisture sources, e.g., Pacific westerlies (Licciardi et al., 2004), and/or (3) more sensitive to temperature (versus precipitation) because of their continental climate (Hostetler and Clark, 1997; Benson et al., 2005). Complex spatial and temporal patterns in glacial response are evident in the western US, and regional differences are often attributed to atmospheric effects related to the Laurentide Ice Sheet. Atmospheric models for LGM climate (Hostetler and Clark, 1997) predict anticyclonic winds off the Laurentide Ice Sheet, which would have affected mountain glaciers proximal to the southern margin of the ice sheet. This anticyclonic circulation would weaken the dominant

westerlies and bring dry air from the east that would reduce precipitation in parts of the region. The glacial chronologies in parts of the western US, e.g., Grand Teton or Yellowstone Plateau, suggest that reduced precipitation strongly affected regional ice dynamics; glacial maxima and retreat were delayed well after the peak of the LGM when the Laurentide Ice Sheet was retreating (15–18 ka, Licciardi et al., 2004; Licciardi and Pierce, 2008).

High pressure over the Laurentide Ice Sheet would also force the polar jet stream and storm tracks southward into the Great Basin (Thompson et al., 1993). Such a shift predicts a drier-than-average climate in the north and wetter conditions in the south. Dia-chronous lake highstands in the Great Basin are thought to indicate a northward sweep of the jet stream caused by the collapse of the Laurentide Ice Sheet (Benson and Thompson, 1987; Oviatt, 1997). These atmospheric patterns would drive changes in water balance, e.g., the extent of lakes, and, in turn, may affect local glacier behavior. For example, Lake Bonneville was a local moisture source for alpine glaciers in the Uinta Mountains whose local maxima and retreat occurred after the LGM (∼16–18 ka, Munroe et al., 2006). Thus, local and regional climate variables, including migrating moisture sources, can cause phase offsets in some glacial systems.

Asynchronous local glacial responses within a mountain range are attributed to spatially variable regional climate forcings. In the northern Rocky Mountains, Licciardi and Pierce (2008) found that the retreat from the Pinedale maximum position varied from 18.8 to 16.5 ka on the Yellowstone Plateau, ∼4–6 ky after glaciers retreated from their maximum position in the adjacent Wind River Range. Differences within the Yellowstone–Teton system may be linked to the spatial pattern of ice accumulation, i.e., southwest-ward propagation of ice buildup, and to differences in internal ice dynamics, whereas differences between Yellowstone and Wind River ranges are related to atmospheric patterns, i.e., the influence of glacial anticyclones.

4.2.3. Comparison to timing and spatial patterns in the western US

Our data permit a broadly synchronous LGM retreat throughout the Sierra Nevada at 18.8 ± 1.9 ka (2σ), which corresponds well with the peak of MIS 2 (discussed further in Section 4.2.4). Our chronology matches patterns of LGM glaciers for some parts of the western United States. Detailed records of glacial fluctuations in the Colorado Rockies (Benson et al., 2005), Wind River Range (Gosse et al., 1995; Licciardi and Pierce, 2008), and Wallowa Mountains (Licciardi et al., 2004) indicate similar retreat from maximum positions attained near the peak of MIS 2.

Our Sierran results differ from several other glacial chronologies in the western United States, e.g., Yellowstone and Tetons (Licciardi and Pierce, 2008) and Uintas (Munroe et al., 2006); in these regions, the LGM retreat appears younger (∼17 ka) by several ky and apparently correlates with the Heinrich event 1 in the northern Atlantic. Direct comparison of our results to published ages from the Cascades is difficult, because they were calculated using the [36]Cl production rates of Swanson and Caffee (2001). Hence, based on the discussion in Section 4.1.2, the calculated Cascadian MIS 2 ages could be ∼30% younger. Porter and Swanson (2008) report an age for Leavenworth II moraines that is younger than MIS 2 (about 16–17 ka, likely corresponding to Heinrich event 1). They give a mean age for the Leavenworth I moraine group of 19.1 ± 3.0 ka (24.7 ± 1.1 ka oldest age), but it is difficult to resolve within these errors whether they correspond with MIS 2, Heinrich event 1, or neither.

Our results indicate less complexity in the regional behavior of glaciers in the Sierra Nevada than is observed at many sites in the western US. The similar pattern of LGM retreat across the 400-km length of the Sierra Nevada suggests these glaciers were not complicated by the Laurentide Ice Sheet, lake, or continentality effects. The regionally consistent pattern among glaciers over

a broad latitude range (36–40°N) suggests consistent climate conditions during the LGM. This similarity in the timing of glacial retreat suggests that a constant regional moisture source, i.e., the Pacific jet stream, sustained Sierra Nevada glaciers during the LGM. For example, we do not recognize any pattern in the response of glaciers that would indicate northward migration of the jet stream inferred from diachronous lake records in the Great Basin (Benson and Thompson, 1987; Oviatt, 1997; Fig. S31). We speculate that the jet stream did not move significantly north of 40°N until after ∼19 ka with the collapse of the Laurentide Ice Sheet.

4.2.4. Comparison to other global and local proxy records

Our Sierran chronology correlates well to some regional and global proxy data, including insolation and global ice volume (Fig. 7). The LGM retreat occurred closely after a minimum in the June insolation for 30°N (Berger and Loutre, 1991), but the corre-lation for the penultimate glaciation is not clear. When compared to global ice volume proxy from marine sediments, the initiation of Sierra Nevada glacial retreats correspond well to global ice volume maxima, and fall within the peaks of MIS 2 and 6 (SPECMAP benthic δ^{18}O curve of Martinson et al., 1987).

Significant differences also exist between our Sierra Nevada chronology and other proxy records. As discussed in Section 4.2.1, no deposits clearly correlate with MIS 4, even though most climate records suggest favorable conditions for glacial activity during this period. Our chronology differs from some regions, e.g., some ranges in Asia (Gillespie and Molnar, 1995; Owen et al., 2008), where MIS 4 moraines are prominent. However, our findings are consistent with other mountain ranges where the landscape is dominated by glacial deposits coeval with MIS 2 and MIS 6, e.g., Yellowstone (Licciardi and Pierce, 2008).

Another difference is that the timing of initial LGM retreat in the Sierra Nevada does not appear to correspond well to air-tempera-ture records in Greenland (GISP2 ice core, Grootes and Stuiver, 1997): a pattern that was identified previously by Schaefer et al. (2006). Such mismatches are difficult to assess, however, when comparisons are made of a discontinuous time series (dated glacial retreat) with a continuous time series (ice core records). Glacial retreats during Heinrich event 1 (∼17 ka), in contrast, appear to be well documented elsewhere and are interpreted to correspond with the local LGM, e.g., Licciardi and Pierce (2008) and Munroe et al. (2006). Whereas isotopic records from Greenland suggest that major post-LGM warming did not initiate until the Bolling interval at 14.7 ka, north Atlantic sediment cores show ice rafting events beginning with Heinrich event 1 at ∼16.8 ka (Hemming, 2004). Phillips et al. (2009) suggest a correspondence between Tioga 4 retreat between 16.9 and 15.8 ka in the Sierra Nevada and Heinrich event 1 in the northern Atlantic. Although they suggest that the Tioga glaciation corresponds with MIS 2 (defined by the authors as 28–14.5 ka), they cite an absence of evidence for glacial events from between 26 and 17.7 ka. Our reevaluation and recal-culation of the Bishop Creek [36]Cl data, and comparison to our [10]Be dataset, improves the resolution with which we can examine correlations with global or regional paleoclimate events, but our study is limited because it focuses on only a few moraines in each catchment, i.e., we did not date inset moraines. Therefore, to the extent that older LGM (pre-Heinrich event 1) events exist else-where (Gosse et al., 1995; Licciardi et al., 2004; Benson et al., 2005; Licciardi and Pierce, 2008), then our data shed little light on whether the Sierra was affected by Heinrich event 1. Our results, however, do not suggest that a correlation is likely between initial LGM retreat of Sierra Nevada glaciers and the peak of warming in Greenland during Heinrich event 1 at 16.8 ka (Hemming, 2004). However, our data could permit such a correlation if one interprets

Heinrich event 1 to include both Heinrich event 1a and 1b between 18 and 15.5 ka (Bard et al., 2000; Denton et al., 2010). Regardless, our data indicate that onset of retreat after the local LGM in the Sierra Nevada was not synchronous with retreat in many ranges of the western US, and preceeded some by several ky.

5. Conclusions

We address the timing and spatial patterns of glaciation in the Sierra Nevada by constructing the first regionally extensive and high-precision chronology using 115 new [10]Be surface exposure dates from Sierran glacial deposits of the last and penultimate glaciations. A compilation of new and published [10]Be and [36]Cl surface exposure ages ($n = 229$) for the Sierra Nevada indicate that Sierra Nevada glaciers retreated from LGM positions at 18.8 ± 1.9 ka (2σ, high confidence sites only). Data from multiple high-resolution chronologies throughout the range permit synchronous retreat of glaciers on the east and west sides of the range, and along the full ~400 km N–S strike. The similarity in glacial response suggests regionally consistent climate changes throughout Sierra Nevada during the LGM. The penultimate glaciation occurred at ca 145 ka (144 ± 14 ka, 2σ, high confidence sites only). The Sierra Nevada landscape is dominated by deposits coeval with MIS 2 and MIS 6; glacial deposits dating to between 25 and 140 ka are not observed, including any associated with MIS 4. Furthermore, [10]Be and [36]Cl chronologies agree within error for Phillips et al.'s (2001) [36]Cl production parameterization, but suggest overestimation of [36]Cl production rates by Swanson and Caffee (2001). Our glacial chronology correlates well with regional paleoclimate records, but indicates initial retreat from local LGM positions several thousand years before many ranges of the western US and likely preceeding warming during the Heinrich event 1.

Acknowledgements

Appendix. Supplementary data

Supplementary data related to this article can be found online at doi:10.1016/j.quascirev.2010.12.001.

References

Amos, C.B., Kelson, K.I., Rood, D.H., Simpson, D.T., Rose, R.S., 2010. Late Quaternary slip rate on the Kern Canyon fault at Soda spring, Tulare County, California. Lithosphere 2 (6), 411–417.

Anderson, R.S., Repka, J.L., Dick, G.S., 1996. Explicit treatment of inheritance in dating depositional surfaces using in situ [10]Be and [26]Al. Geology 24 (1), 47–51.

Anderson, R.S., Molnar, P., Kessler, M.A., 2006. Features of glacial valley profiles simply explained. Journal of Geophysical Research 111 (F1), F01004.

Balco, G., Stone, J.O., Lifton, N.A., Dunai, T.J., 2008. A complete and easily accessible means of calculating surface exposure ages or erosion rates from [10]Be and [26]Al measurements. Quaternary Geochronology 3 (3), 174–195.

Balco, G., Briner, J., Finkel, R.C., Rayburn, J.A., Ridge, J.C., Schaefer, J.M., 2009. Regional beryllium-10 production rate calibration for late-glacial northeastern North America. Quaternary Geochronology 4 (2), 93–107.

Bard, E., Rostek, F., Turon, J., Gendreau, S., 2000. Hydrological impact of Heinrich events the subtropical northeast Atlantic. Science 289, 1321–1324.

Bartlein, P.J., Anderson, K.H., Anderson, P.M., Edwards, M.E., Mock, C.J., Thompson, R.S., Webb, R.S., Webb, T., Whitlock, C., 1998. Paleoclimate simulations for North America over the past 21,000 years: features of the simulated climate and comparisons with paleoenvironmental data. Quaternary Science Reviews 17 (6–7), 549–585.

Benedict, J.B., 1993. Influence of snow upon rates of granodiorite weathering, Colorado Front Range, USA. Boreas 22 (2), 87–92.

Benn, D.I., Owen, L.A., Finkel, R.C., Clemmens, S., 2006. Pleistocene lake outburst floods and fan formation along the eastern Sierra Nevada, California: implications for the interpretation of intermontane lacustrine records. Quaternary Science Reviews 25 (21–22), 2729–2748.

Benson, L.V., Thompson, R.S., 1987. Lake-level variation in the Lahontan basin for the past 50,000 years. Quaternary Research 28 (1), 69–85.

Benson, L., Lund, S., Negrini, R., Linsley, B., Zic, M., 2003. Response of north American Great basin lakes to Dansgaard–Oeschger oscillations. Quaternary Science Reviews 22 (21–22), 2239–2251.

Benson, L., Madole, R., Landis, G., Gosse, J., 2005. New data for Late Pleistocene Pinedale alpine glaciation from southwestern Colorado. Quaternary Science Reviews 24 (1–2), 49–65.

Berger, A., Loutre, M.F., 1991. Insolation values for the climate of the last 10 million years. Quaternary Science Reviews 10 (4), 297–317.

Bierman, P., Gillespie, A., 1991. Range fires: a significant factor in exposure-age determination and geomorphic surface evolution. Geology 19 (6), 641–644.

Bischoff, J.L., Cummins, K., 2001. Wisconsin glaciation of the Sierra Nevada (79,000–15,000 yr B.P.) as recorded by rock flour in sediments of Owens Lake, California. Quaternary Research 55 (1), 14–24.

Bischoff, J.L., Menking, K.M., Fitts, J.P., Fitzpatrick, J.A., 1997. Climatic oscillations 10,000–155,000 yr B.P. at Owens Lake, California Reflected in glacial rock flour abundance and lake salinity in core OL-92. Quaternary Research 48 (3), 313–325.

Blackwelder, E., 1931. Pleistocene glaciation in the Sierra Nevada and basin ranges. Geological Society of America Bulletin 42 (4), 865–922.

Briner, J.P., Kaufman, D.S., 2008. Late Pleistocene mountain glaciation in Alaska: key chronologies. Journal of Quaternary Science 23 (6–7), 659–670.

Burbank, D.W., 1991. Late Quaternary snowline reconstructions for the southern and central Sierra Nevada, California and a reassessment of the "recess peak glaciation". Quaternary Research 36 (3), 294–306.

Burke, R.M., Birkeland, P.W., 1979. Reevaluation of multiparameter relative dating techniques and their application to the glacial sequence along the eastern escarpment of the Sierra Nevada, California. Quaternary Research 11 (1), 21–51.

Bursik, M. I. 1989. Late Quaternary volcano-tectonic evolution of the Mono Basin, eastern California. Unpublished doctoral thesis, California Institute of Technology.

Bursik, M.I., Gillespie, A.R., 1993. Late Pleistocene glaciation of Mono basin, California. Quaternary Research 39 (1), 24–35.

Chmeleff, J., von Blanckenburg, F., Kossert, K., Jakob, D., 2010. Determination of the [10]Be half-life by multicollector ICP-MS and liquid scintillation counting. Nuclear Instruments and Methods in Physics Research Section B: Beam Interactions with Materials and Atoms 268 (2), 192–199.

Clark, M. 1967. Pleistocene glaciation of the drainage of the West Walker River, Sierra Nevada, California. Unpublished doctoral thesis, Stanford University.

Clark, D.H., Gillespie, A.R., 1997. Timing and significance of late-glacial and Holocene cirque glaciation in the Sierra Nevada, California. Quaternary International 38–39, 21–38.

Clark, D., Gillespie, A.R., Clark, M.M., Burke, B., 2003. Mountain Glaciations of the Sierra Nevada. Desert Research Institute, Reno, NV, United States (USA).

Clark, P.U., Dyke, A.S., Shakun, J.D., Carlson, A.E., Clark, J., Wohlfarth, B., Mitrovica, J.X., Hostetler, S.W., McCabe, A.M., 2009. The last glacial maximum. Science 325 (5941), 710–714.

Denton, G.H., Anderson, R.F., Toggweiler, J.R., Edwards, R.L., Schaefer, J.M., Putnam, A.E., 2010. The last glacial termination. Science 328, 1652–1656.

Desilets, D., Zreda, M., Prabu, T., 2006. Extended scaling factors for in situ cosmogenic nuclides: new measurements at low latitude. Earth and Planetary Science Letters 246 (3–4), 265–276.

Dunai, T.J., 2001. Influence of secular variation of the geomagnetic field on production rates of in situ produced cosmogenic nuclides. Earth and Planetary Science Letters 193 (1–2), 197–212.

Gibbons, A.B., Megeath, J.D., Pierce, K.L., 1984. Probability of moraine survival in a succession of glacial advances. Geology 12 (6), 327–330.

Gillespie, A.R., 1982. Quaternary Glaciation and Tectonism in the Southeastern Sierra Nevada Inyo County, California.

Gillespie, A., Molnar, P., 1995. Asynchronous maximum advances of mountain and continental glaciers. Reviews of Geophysics 33 (3), 311–364.

Gillespie, A.R., Clark, M.M., Burke, R.M., 1999. Eliot Blackwelder and the alpine glaciations of the Sierra Nevada. In: Geological Society of America Special Paper, vol. 338, pp. 443–452.

Gosse, J.C., Phillips, F.M., 2001. Terrestrial in situ cosmogenic nuclides: theory and application. Quaternary Science Reviews 20 (14), 1475–1560.

Gosse, J.C., Klein, J., Evenson, E.B., Lawn, B., Middleton, R., 1995. Beryllium-10 dating of the duration and retreat of the last Pinedale glacial sequence. Science 268 (5215), 1329–1333.

Grootes, P.M., Stuiver, M., 1997. Oxygen 18/16 variability in Greenland snow and ice with 10^{-3} to 10^5 year time resolution. Journal of Geophysical Research 102 (c12), 26455–26526.

Guilderson, T.P., Southon, J.R., Brown, T.A., 2003. High-precision AMS ^{14}C results on TIRI/FIRI turbidite. Radiocarbon 45 (1), 75–80.

Hein, A.S., Hulton, NR.J., Dunai, T.J., Schnabel, C., Kaplan, M.R., Naylor, M., Xu, S., 2009. Middle Pleistocene glaciation in Patagonia dated by cosmogenic-nuclide measurements on outwash gravels. Earth and Planetary Science Letters 286, 184–197.

Heisinger, B., Lal, D., Jull, A.J.T., Kubik, P., Ivy-Ochs, S., Knie, K., Nolte, E., 2002a. Production of selected cosmogenic radionuclides by muons: 2. Capture of negative muons. Earth and Planetary Science Letters 200 (3–4), 357–369.

Heisinger, B., Lal, D., Jull, A.J.T., Kubik, P., Ivy-Ochs, S., Neumaier, S., Knie, K., Lazarev, V., Nolte, E., 2002b. Production of selected cosmogenic radionuclides by muons: 1. Fast muons. Earth and Planetary Science Letters 200 (3–4), 345–355.

Hemming, S.R., 2004. Heinrich events: massive late Pleistocene detritus layers of the North Atlantic and their global climate imprint. Reviews of Geophysics 42 (1), RG1005.

Hostetler, S.W., Clark, P.U., 1997. Climatic controls of Western U.S. glaciers at the last glacial maximum. Quaternary Science Reviews 16 (6), 505–511.

Howat, I.M., Tulaczyk, S., 2005. Climate sensitivity of spring snowpack in the Sierra Nevada. Journal of Geophysical Research 110 (F4), F04021.

Huybers, K., Roe, G.H., 2009. Spatial patterns of glaciers in response to spatial patterns in regional climate. Journal of Climate 22 (17), 4606–4620.

James, L.A., Harbor, J., Fabel, D., Dahms, D., Elmore, D., 2002. Late Pleistocene glaciations in the Northwestern Sierra Nevada, California. Quaternary Research 57 (3), 409–419.

Kessler, M.A., Anderson, R.S., Stock, G.M., 2006. Modeling topographic and climatic control of east–west asymmetry in Sierra Nevada glacier length during the last glacial maximum. Journal of Geophysical Research 111 (F2), F02002.

Kirby, E., Burbank, D.W., Reheis, M., Phillips, F, 2006. Temporal variations in slip rate of the White Mountain Fault Zone, Eastern California. Earth and Planetary Science Letters 248 (1–2), 168–185.

Kohfeld, K.E., Harrison, S.P., 2000. How well can we simulate past climates? Evaluating the models using global palaeoenvironmental datasets. Quaternary Science Reviews 19 (1–5), 321–346.

Korschinek, G., Bergmaier, A., Faestermann, T., Gerstmann, U.C., Knie, K., Rugel, G., Wallner, A., Dillmann, I., Dollinger, G., von Gostomski, C.L., Kossert, K., Maiti, M., Poutivtsev, M., Remmert, A., 2010. A new value for the half-life of ^{10}Be by heavy-ion elastic recoil detection and liquid scintillation counting. Nuclear Instruments and Methods in Physics Research Section B: Beam Interactions with Materials and Atoms 268 (2), 187–191.

Lal, D., 1991. Cosmic ray labeling of erosion surfaces: in situ nuclide production rates and erosion models. Earth and Planetary Science Letters 104 (2–4), 424–439.

Licciardi, J.M., Pierce, K.L., 2008. Cosmogenic exposure-age chronologies of Pinedale and Bull Lake glaciations in greater Yellowstone and the Teton range, USA. Quaternary Science Reviews 27 (7–8), 814–831.

Licciardi, J.M., Clark, P.U., Brook, E.J., Elmore, D., Sharma, P., 2004. Variable responses of western U.S. glaciers during the last deglaciation. Geology 32 (1), 81–84.

Lifton, N., Caffee, M.W., Finkel, R., Schaefer, J.M., Stone, J., Goehring, B.M., Phillips, F., Oviatt, C.G., Rood, D.H., 2009. A new estimate of the spallogenic production rate of in situ cosmogenic ^{10}Be from Lake Bonneville shoreline features, Promontory Point, Utah. Geological Society of America Abstracts with Programs 41 (7), 229.

Lifton, N.A., Bieber, J.W., Clem, J.M., Duldig, M.L., Evenson, P., Humble, J.E., Pyle, R., 2005. Addressing solar modulation and long-term uncertainties in scaling secondary cosmic rays for in situ cosmogenic nuclide applications. Earth and Planetary Science Letters 239 (1–2), 140–161.

Litwin, R.J., Smoot, J.P., Durika, N.J., Smith, G.I., 1999. Calibrating Late Quaternary terrestrial climate signals: radiometrically dated pollen evidence from the southern Sierra Nevada, USA. Quaternary Science Reviews 18 (10–11), 1151–1171.

Martinson, D.G., Pisias, N.G., Hays, J.D., Imbrie, J., Moore, T.C., Shackleton, N.J., 1987. Age dating and the orbital theory of the ice ages: development of a high-resolution 0 to 300,000-year chronostratigraphy. Quaternary Research 27 (1), 1–29.

Menking, K.M., Bischoff, J.L., Fitzpatrick, J.A., Burdette, J.W., Rye, R.O., 1997. Climatic/hydrologic oscillations since 155,000 yr B.P. at Owens Lake, California, reflected in abundance and stable isotope composition of sediment carbonate. Quaternary Research 48 (1), 58–68.

Merchel, S., Arnold, M., Aumaître, G., Benedetti, L., Bourlès, D.L., Braucher, R., Alfimov, V., Freeman, S.P.H.T., Steier, P., Wallner, A., 2008. Towards more precise ^{10}Be and ^{36}Cl data from measurements at the 10^{-14} level: influence of sample preparation. Nuclear Instruments and Methods in Physics Research Section B: Beam Interactions with Materials and Atoms 266 (22), 4921–4926.

Mix, A.C., Bard, E., Schneider, R., 2001. Environmental processes of the ice age: land, oceans, glaciers (EPILOG). Quaternary Science Reviews 20 (4), 627–657.

Munroe, J.S., Laabs, B.J.C., Shakun, J.D., Singer, B.S., Mickelson, D.M., Refsnider, K.A., Caffee, M.W., 2006. Latest Pleistocene advance of alpine glaciers in the south-western Uinta Mountains, Utah, USA: evidence for the influence of local moisture sources. Geology 34 (10), 841–844.

Nichols, K.K., Bierman, P.R., Foniri, W.R., Gillespie, A.R., Caffee, M., Finkel, R., 2006. Dates and rates of arid region geomorphic processes from analysis of cosmogenic nuclides. GSA Today 16 (8), 4–11.

Nishiizumi, K., Imamura, M., Caffee, M.W., Southon, J.R., Finkel, R.C., McAninch, J., 2007. Absolute calibration of ^{10}Be AMS standards. Nuclear Instruments and Methods in Physics Research Section B: Beam Interactions with Materials and Atoms 258 (2), 403–413.

Oerlemans, J., 2005. Extracting a climate signal from 169 glacier records. Science 308 (5722), 675–677.

Oviatt, C.G., 1997. Lake Bonneville fluctuations and global climate change. Geology 25 (2), 155–158.

Owen, L.A., Caffee, M.W., Finkel, R.C., Seong, Y.B., 2008. Quaternary glaciation of the Himalayan–Tibetan orogen. Journal of Quaternary Science 23 (6–7), 513–531.

Owen, L.A., Thackray, G., Anderson, R.S., Briner, J., Kaufman, D., Roe, G., Pfeffer, W., Yi, C., 2009. Integrated research on mountain glaciers: current status, priorities and future prospects. Geomorphology 103 (2), 158–171.

Perg, L.A., Anderson, R.S., Finkel, R.C., 2001. Use of a new ^{10}Be and ^{26}Al inventory method to date marine terraces, Santa Cruz, California, USA. Geology 29 (10), 879–882.

Phillips, F.M., Zreda, M.G., Smith, S.S., Elmore, D., Kubik, P.W., Sharma, P., 1990. Cosmogenic chlorine-36 chronology for glacial deposits at Bloody Canyon, eastern Sierra Nevada. Science 248 (4962), 1529–1532.

Phillips, F.M., Zreda, M.G., Benson, L.V., Plummer, M.A., Elmore, D., Sharma, P., 1996. Chronology for fluctuations in late Pleistocene Sierra Nevada glaciers and lakes. Science 274 (5288), 749–751.

Phillips, F.M., Zreda, M.G., Gosse, J.C., Klein, J., Evenson, E.B., Hall, R.D., Chadwick, O.A., Sharma, P., 1997. Cosmogenic ^{36}Cl and ^{10}Be ages of Quaternary glacial and fluvial deposits of the wind River range, Wyoming. Geological Society of America Bulletin 109 (11), 1453–1463.

Phillips, F.M., Stone, W.D., Fabryka-Martin, J.T., 2001. An improved approach to calculating low-energy cosmic-ray neutron fluxes near the land/atmosphere interface. Chemical Geology 175 (3–4), 689–701.

Phillips, F.M., Zreda, M., Plummer, M.A., Elmore, D., Clark, D.H., 2009. Glacial geology and chronology of Bishop Creek and vicinity, eastern Sierra Nevada, California. Geological Society of America Bulletin 121 (7–8), 1013–1033.

Pigati, J.S., Zreda, M., Zweck, C., Almasi, P.F., Elmore, D., Sharp, W.D., 2008. Ages and inferred causes of late Pleistocene glaciations on Mauna Kea, Hawai'i. Journal of Quaternary Science 23 (6–7), 683–702.

Porter, S.C., 2001. Snowline depression in the tropics during the last glaciation. Quaternary Science Reviews 20 (10), 1067–1091.

Porter, S.C., Swanson, T.W., 2008. (super 36) Cl dating of the classic Pleistocene glacial record in the northeastern Cascade range, Washington. The American Journal of Science 308 (2), 130–166.

Putkonen, J., O'Neal, M., 2006. Degradation of unconsolidated Quaternary landforms in the western North America. Geomorphology 75 (3–4), 408–419.

Putkonen, J., Swanson, T., 2003. Accuracy of cosmogenic ages for moraines. Quaternary Research 59 (2), 255–261.

Putnam, A.E., Schaefer, J.M., Barrell, D.J.A., Vandergoes, M., Denton, G.H., Kaplan, M.R., Finkel, R.C., Schwartz, R., Goehring, B.M., Kelley, S.E., 2010. In situ cosmogenic ^{10}Be production rate calibration from the Southern Alps, New Zealand. Quaternary Geochronology 5, 392–409.

Ramelli, A.R., Bell, J.W., dePolo, C.M., Yount, J.C., 1999. Large-magnitude, late Holocene earthquakes on the Genoa fault, west-central Nevada and eastern California. Bulletin of the Seismological Society of America 89 (6), 1458–1472.

Rood, D.H., Hall, S., Guilderson, T.P., Finkel, R.C., Brown, T.A., 2010. Challenges and opportunities in high-precision Be-10 measurements at CAMS. Nuclear Instruments and Methods in Physics Research Section B: Beam Interactions with Materials and Atoms 268 (7–8), 730–732.

Rood, D.H., Burbank, D.W., Finkel, R.C., 2011. Spatiotemporal patterns of fault slip rates across the central Sierra Nevada Frontal Fault Zone. Earth and Planetery Science Letters 301, 457–468. doi:10.1016/j.epsl.2010.11.006.

Schaefer, J.M., Denton, G.H., Barrell, D.J.A., Ivy-Ochs, S., Kubik, P.W., Andersen, B.G., Phillips, F.M., Lowell, T.V., Schluchter, C., 2006. Near-synchronous interhemispheric termination of the last glacial maximum in mid-latitudes. Science 312 (5779), 1510–1513.

Schaefer, J.M., Denton, G.H., Kaplan, M., Putnam, A., Finkel, R.C., Barrell, D.J.A., Andersen, B.G., Schwartz, R., Mackintosh, A., Chinn, T., Schluchter, C., 2009. High-frequency Holocene glacier fluctuations in New Zealand Differ from the northern signature. Science 324 (5927), 622–625.

Schimmelpfennig, I., Benedetti, L., Finkel, R., Pik, R., Blard, P.-H., Bourlès, D., Burnard, P., Williams, A., 2009. Sources of in-situ ^{36}Cl in basaltic rocks. Implications for calibration of production rates. Quaternary Geochronology 4 (6), 441–461.

Sharp, R.P., 1972. Pleistocene glaciation, Bridgeport basin, California. Geological Society of America Bulletin 83 (8), 2233–2260.

Sharp, R.P., Birman, J.H., 1963. Additions to classical sequence of Pleistocene glaciations, Sierra Nevada, California. Geological Society of America Bulletin 74 (8), 1079–1086.

Small, E.E., Anderson, R.S., Repka, J.L., Finkel, R., 1997. Erosion rates of alpine bedrock summit surfaces deduced from in situ ^{10}Be and ^{26}Al. Earth and Planetary Science Letters 150 (3–4), 413–425.

Smith, J.A., Finkel, R.C., Farber, D.L., Rodbell, D.T., Seltzer, G.O., 2005. Moraine preservation and boulder erosion in the tropical Andes: interpreting old surface

exposure ages in glaciated valleys. Journal of Quaternary Science 20 (7–8), 735–758.

Smith, J.A., Mark, B.G., Rodbell, D.T., 2008. The timing and magnitude of mountain glaciation in the tropical Andes. Journal of Quaternary Science 23 (6–7), 609–634.

Stone, J.O., 2000. Air pressure and cosmogenic isotope production. Journal of Geophysical Research 105 (b10), 23753–23823.

Stone, J., Evans, J., Fifield, K., Cresswell, R., Allan, G., 1996a. Cosmogenic chlorine-36 production rates from calcium and potassium. Radiocarbon 38 (1), 170–171.

Stone, J.O., Allan, G.L., Fifield, L.K., Cresswell, R.G., 1996b. Cosmogenic chlorine-36 from calcium spallation. Geochimica et Cosmochimica Acta 60 (4), 679–692.

Swanson, T.W., Caffee, M.L., 2001. Determination of ^{36}Cl production rates derived from the well-dated deglaciation surfaces of Whidbey and Fidalgo Islands, Washington. Quaternary Research 56 (3), 366–382.

Thackray, G.D., Owen, L.A., Yi, C., 2008. Timing and nature of late Quaternary mountain glaciation. Journal of Quaternary Science 23 (6–7), 503–508.

Thompson, R.S., Whitlock, C., Bartlein, P.J., Harrison, S.P., Spaulding, W.G., 1993. Climatic changes in the western United States since 18,000 yr B.P. In: Wright, H.E., Kutzbach, J.E., Webb T. III, Ruddiman, W.F., Street-Perrott, F.A., Bartlein, P.J. (Eds.), Global Climates Since the Last Glacial Maximum. University of Minnesota Press, Minneapolis, MN, pp. 468–513.

Warhaftig, C., Birman, J.H., 1965. The Quaternary of the Pacific mountain system in California. In: Wright H.E. Jr, Frey, D.G. (Eds.), The Quaternary of the United States. Princeton University Press, Princeton, New Jersey, pp. 299–340.

Winograd, I.J., Landwehr, J.M., Coplen, T.B., Sharp, W.D., Riggs, A.C., Ludwig, K.R., Kolesar, P.T., 2006. Devils Hole, Nevada, δ^{18}O record extended to the mid-Holocene. Quaternary Research 66 (2), 202–212.

Winograd, I.J., Landwehr, J.M., Ludwig, K.R., Coplen, T.B., Riggs, A.C., 1997. Duration and structure of the past four interglaciations. Quaternary Research 48, 141–154.

Yamamoto, M., Yamamuro, M., Tanaka, Y., 2007. The California current system during the last 136,000 years: response of the north Pacific high to precessional forcing. Quaternary Science Reviews 26 (3–4), 405–414.